

# Chapter 2

## Fractional Order PID and First Generation CRONE Control System Design

P. Lanusse, J. Sabatier, and A. Oustaloup

This chapter presents the design of controllers for Single Input/Single Output (SISO) systems, that is to say only one signal to control only one measured output. The fractional order controller is presented as a generalization of the common PID controller. Then, it is shown how the first generation of the CRONE methodology is able to design robust controllers for a class of gain-like perturbed systems.

### 2.1 Output Feedback Control System

Two kinds of models can be used to model dynamic systems: state space models and transfer functions (when a linear time invariant model is sufficient). All the proposed control system design methodologies presented here use transfer function modeling of the *plant* (the system to be controlled) and an output unity negative feedback control system (Fig. 2.1). Furthermore, in the fractional order framework, a state space feedback control system is not so easy to use as it requires the fractional-order state space vector of the plant which is not available most of the time.

In Fig. 2.1:

- $G$  is the plant,  $G(s)$  the transfer function of its linear model,  $u(t)$  its control effort input,  $y(t)$  its output to be controlled and  $y_{\text{mes}}(t)$  its measure;
- $C(s)$  is the linear controller providing the control effort  $u(t)$ ;
- $y_{\text{ref}}(t)$  is the reference (desired) value of output  $y(t)$ ;
- $d_u(t)$  is a disturbance on the plant input;

---

P. Lanusse (✉) • J. Sabatier • A. Oustaloup

IMS Laboratory - CNRS UMR 5218 – Bordeaux INP - Bordeaux University Bat A31 – 351 cours de la Libération, 33400, Cedex Talence, France

e-mail: [Patrick.Lanusse@ims-bordeaux.fr](mailto:Patrick.Lanusse@ims-bordeaux.fr)

© Springer Science+Business Media Dordrecht 2015

J. Sabatier et al. (eds.), *Fractional Order Differentiation and Robust*

*Control Design*, Intelligent Systems, Control and Automation:

Science and Engineering 77, DOI 10.1007/978-94-017-9807-5\_2

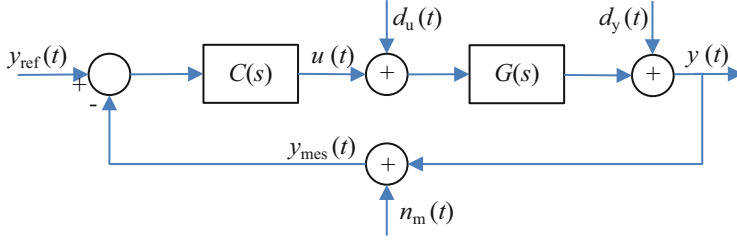


**Fig. 2.1** Block-diagram of an output unity negative feedback control system

- $d_y(t)$  is a disturbance on the plant output;
- $n_m(t)$  is a high-frequency measurement noise.

### 2.1.1 Closed-Loop Transfer and Sensitivity Functions

Several closed-loop transfer functions between the Laplace transform of the input and output signals of the feedback control-system of Fig. 2.1 can be written:

$$T(s) = \frac{Y_{\text{mes}}(s)}{Y_{\text{ref}}(s)} = -\frac{Y_{\text{mes}}(s)}{N_m(s)} = -\frac{U(s)}{P_u(s)} = \frac{G(s)C(s)}{1 + G(s)C(s)}; \quad (2.1)$$

$$S(s) = \frac{Y_{\text{mes}}(s)}{P_y(s)} = \frac{1}{1 + G(s)C(s)}; \quad (2.2)$$

$$SG(s) = \frac{Y_{\text{mes}}(s)}{P_u(s)} = \frac{G(s)}{1 + G(s)C(s)}; \quad (2.3)$$

$$CS(s) = \frac{U(s)}{Y_{\text{ref}}(s)} = -\frac{U(s)}{N_m(s)} = -\frac{U(s)}{P_y(s)} = \frac{C(s)}{1 + C(s)G(s)}. \quad (2.4)$$

$S(s)$  is also defined by:

$$S(s) = \frac{\partial T(s)}{T(s)} / \frac{\partial G(s)}{G(s)}, \quad (2.5)$$

where  $\partial T(s)/T(s)$  and  $\partial G(s)/G(s)$  are the relative uncertainty of  $T(s)$  and  $G(s)$ . The plant uncertainty (or perturbation) comes from variations in its model and/or its parameters. As  $S(s)$  measures the desensitization of the output/input gain versus the plant uncertainty which is provided by the closed-loop control system, it is called the *sensitivity transfer function*. Thus as

$$T(s) = 1 - S(s), \quad (2.6)$$

$T(s)$  is called the *complementary sensitivity function*. By extension, as  $SG(s)$  is relative to the input disturbance, it is called the *input sensitivity function*, and,  $CS(s)$ , which is relative to the control effort, is called the *control sensitivity function*.

As the plant output has to converge to a reference value, for low frequency (long durations) the complementary sensitivity function has to be close to one within this frequency range, and thus the magnitude of the open-loop transfer function  $\beta = GC$  needs to be much greater than one:

$$|G(j\omega) C(j\omega)| \gg 1 \Rightarrow |T(j\omega)| = \left| \frac{G(j\omega) C(j\omega)}{1 + G(j\omega) C(j\omega)} \right| \approx 1. \quad (2.7)$$

As the plant output has to be as independent as possible from the measurement noise, for high frequency (short durations) the complementary sensitivity function has to be close to zero within this frequency range, and thus the magnitude of the open-loop transfer function  $\beta = GC$  needs to be small:

$$|G(j\omega) C(j\omega)| \ll 1 \Rightarrow |T(j\omega)| = \left| \frac{G(j\omega) C(j\omega)}{1 + G(j\omega) C(j\omega)} \right| \approx |G(j\omega) C(j\omega)| \ll 1. \quad (2.8)$$

Figure 2.2 depicts the magnitude of the frequency response of the complementary sensitivity function  $T$  for a plant  $G$  and a controller  $C$ . The (0 dB) gain crossover frequency  $\omega_{cg}$  of the open-loop transfer function  $\beta$  is very close to the (-3 dB) cut-off frequency  $\omega_c$  of the closed-loop transfer function  $T$ :

$$\omega_{cg} \approx \omega_c \text{ with } \begin{cases} |G(j\omega_{cg}) C(j\omega_{cg})| = 1 \\ |T(j\omega_c)| = 1/\sqrt{2} \end{cases}. \quad (2.9)$$

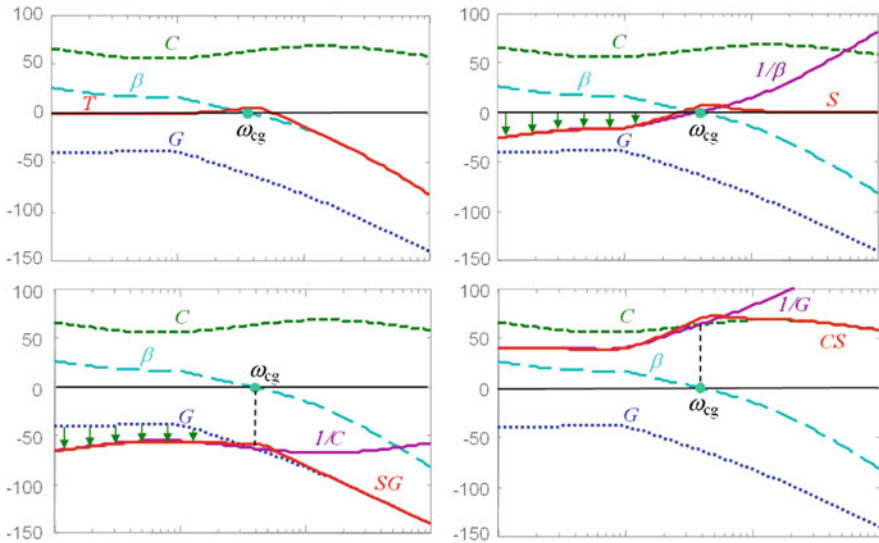


**Fig. 2.2** Magnitude of the four closed-loop sensitivity functions  $T$ ,  $S$ ,  $SG$ ,  $CS$  for given  $G$  and  $C$

Figure 2.2 shows that the frequency range within which the output plant is less sensitive ( $|S(j\omega)| < 1$ ) both to the plant uncertainty and to an output disturbance is limited by  $\omega_{cg}$ :

$$|S(j\omega)| = \left| \frac{1}{1 + G(j\omega) C(j\omega)} \right| < 1 \Rightarrow |G(j\omega) C(j\omega)| > 1 \Rightarrow \omega < \omega_{cg}. \quad (2.10)$$

For frequencies higher than  $\omega_{cg}$ , the sensitivity function  $S$  is close to 1

$$|G(j\omega) C(j\omega)| < 1 \Rightarrow |S(j\omega)| = \left| \frac{1}{1 + G(j\omega) C(j\omega)} \right| \approx 1 \quad (2.11)$$

meaning that no desensitization is provided over  $\omega_{cg}$ . The same holds for the input sensitivity function  $SG$ . Furthermore, the greater the magnitude of the controller, the more efficient the rejection of the input disturbance for frequencies lower than  $\omega_{cg}$ :

$$|G(j\omega) C(j\omega)| > 1 \Rightarrow |SG(j\omega)| = \left| \frac{G(j\omega)}{1 + G(j\omega) C(j\omega)} \right| \approx \left| \frac{1}{C(j\omega)} \right|. \quad (2.12)$$

For frequencies higher than  $\omega_{cg}$ , the sensitivity function  $SG$  remains close to  $G$

$$|G(j\omega) C(j\omega)| < 1 \Rightarrow |SG(j\omega)| = \left| \frac{G(j\omega)}{1 + G(j\omega) C(j\omega)} \right| \approx |G(j\omega)| \quad (2.13)$$

meaning that the input disturbance is not rejected over  $\omega_{cg}$ .

Figure 2.2 shows that the control sensitivity function is close to  $C$  for frequencies greater than  $\omega_{cg}$ :

$$|G(j\omega) C(j\omega)| < 1 \Rightarrow |CS(j\omega)| = \left| \frac{C(j\omega)}{1 + G(j\omega) C(j\omega)} \right| \approx |C(j\omega)|. \quad (2.14)$$

This means that the larger the controller gain, the more amplified the high frequency components of the reference output and of the measurement noise will be.

### 2.1.2 Control System Performance

The bandwidth of the closed-loop system can be defined by the cut-off frequency  $\omega_c$  which is close to  $\omega_{cg}$ . For a step variation of  $y_{ref}$ , using a rule of thumb, the rise time (time taken by  $y$  to change from 10 % to 90 % of its variation) can be

$$t_r \approx \frac{2}{\omega_c} \quad (2.15)$$

for well-damped closed-loop systems. The settling time (time taken by  $y$  to reach and stay within a range from 95 % to 105 % of its variation) is such that

$$t_s \geq \frac{3}{\omega_c}. \quad (2.16)$$

Like the time needed for the desensitization of the plant output to disturbances and plant uncertainty, the larger  $\omega_{cg}$  is, the smaller  $t_r$  and  $t_s$  are. Thus, the open-loop gain cross-over frequency  $\omega_{cg}$  is often used as a design parameter to ensure a given dynamic (bandwidth) to the closed-loop system.

As physical plants are modeled by decreasing the magnitude with respect to the frequency, the definition of  $\omega_{cg}$  (2.9) expresses that the higher  $\omega_{cg}$  is, the higher the required magnitude of  $C$  for  $\omega_{cg}$ :

$$|C(j\omega_{cg})| = \frac{1}{|G(j\omega_{cg})|}. \quad (2.17)$$

Relations (2.1), (2.2), (2.3), (2.7), (2.10) and (2.11) show that the higher the magnitude of  $C$ , the more accurate the tracking of the reference value of  $y_{ref}$  by  $y$  and the more efficient the rejection of input and output disturbances.

Conversely, (2.4) and (2.14) show that a large gain of  $C$  can dramatically amplify the high frequency components of the reference output and of the measurement noise. Thus, the design of a controller requires managing the tradeoff between the bandwidth it tries to ensure and the control effort it is allowed to provide. Taking into account the magnitude of the high-frequency measurement noise  $|n_m|$ , the greatest admissible magnitude of the control-effort noise  $\max|u_{nm}|$ , and relations (2.4) and (2.14), the high-frequency magnitude of  $|C(j\omega)|_{HF}$  should be such that:

$$|C(j\omega)|_{HF} \leq \frac{\max|u_{nm}|}{|n_m|}. \quad (2.18)$$

As  $\max|u_{nm}|$  is often defined by 10 % of  $u_{SAT}$ , the saturated value of  $u(t)$ , if  $C(s)$  is a proportional controller defined by  $C(s) = C_0$ , (2.17) and (2.18) lead to:

$$|G(j\omega_{cg})| \geq \frac{0.1|n_m|}{u_{SAT}}. \quad (2.19)$$

This relation expresses that  $\omega_{cg}$  should not exceed the frequency at which the magnitude of  $G(j\omega)$  equals a given factor of  $|n_m|/u_{SAT}$ .

## 2.2 Feedforward Control System

Even if a feedback control system can ensure perfect tracking of the reference value  $y_{ref}$  by  $y$ , taking into account the bandwidth/control effort tradeoff, the settling time of  $y$  is sometimes not as short as possible. Thus, to reduce this settling time, a

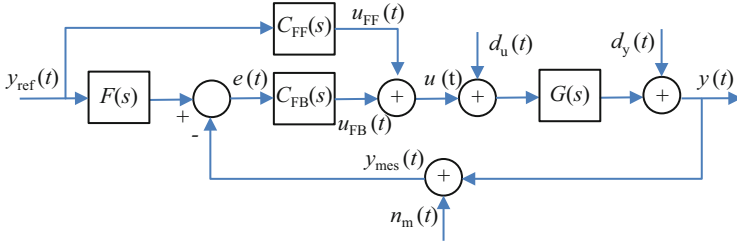


**Fig. 2.3** Block-diagram of an output unity negative feedback and of a feedforward control system

feedforward control system can be used when the behavior of the plant is sufficiently well known (Fig. 2.3).

In Fig. 2.3:

- $C_{FF}(s)$  is the transfer function of a feedforward filter;
- $F(s)$  is a linear prefilter;
- $C_{FB}(s)$  is the feedback controller presented above.

Let  $\tilde{G}(s)$  be a reduced-order model (that does not model a high-frequency behavior) of the nominal transfer function  $G_{nom}(s)$  of the plant. The feedforward filter can then be defined by

$$C_{FF}(s) = \tilde{G}^{-1}(s)H(s), \quad (2.20)$$

where the filter  $H(s)$  is a unity-static gain transfer function that has to:

- lead to the reachable settling time with a suitable dynamic;
- make  $C_{FF}(s)$  proper (biproper or strictly-proper);
- provide a control effort  $u_{FF}(t)$  that satisfies the limitations on the plant control-effort.

Thus,  $y(t)$  comes close to  $y_{ref}(t)$  with the dynamic of  $H(s)$  and the control effort  $u(t)$  is directly set to  $u_{FF}(t)$  without the need for convergence time. Nevertheless, as the plant is perturbed ( $G(s) \neq G_{nom}(s)$ ), as the feedforward model differs from the nominal plant ( $\tilde{G}(s) \neq G_{nom}(s)$ ), and as the disturbances are not perfectly known, a feedback control system needs to be associated to reduce the error signal  $e(t)$ .

The prefilter transfer function is designed such that the error signal will be null if  $G(s)$  equals  $G_{nom}(s)$  and whatever the value of  $C(s)$ :

$$F(s) = G_{nom}(s)C_{FF}(s). \quad (2.21)$$

The transfer function between the reference and measured values of  $y$  is now:

$$\frac{Y_{mes}(s)}{Y_{ref}(s)} = \frac{G(s)(1 + C_{FB}(s)G_{nom}(s))C_{FF}(s)}{1 + G(s)C_{FB}(s)}. \quad (2.22)$$

If the magnitude of the open-loop is much greater than 1 within a given frequency range, then:

$$\left| \frac{Y_{\text{mes}}(j\omega)}{Y_{\text{ref}}(j\omega)} \right| \xrightarrow{\substack{|C_{\text{FB}}(j\omega) G_{\text{nom}}(j\omega)| \gg 1 \\ |G(j\omega) C_{\text{FB}}(j\omega)| \gg 1}} |G_{\text{nom}}(j\omega) C_{\text{FF}}(j\omega)| = |G_{\text{nom}}(j\omega) \tilde{G}^{-1}(j\omega) H(j\omega)|. \quad (2.23)$$

As the gain of (2.23) tends to 1 in low frequency, it shows that the feedback controller  $C_{\text{FB}}(s)$  is able to provide the complementary control effort  $u_{\text{FB}}(t)$  to ensure the perfect convergence of  $y(t)$  to  $y_{\text{ref}}(t)$ .

## 2.3 Stability Margins and Robustness

### 2.3.1 Stability Margins

It is obvious that the output of the closed-loop system is able to converge with its reference value only if the closed-loop system is stable. It is well known that the stability of a transfer function can be stated by analyzing its poles that have to be with a negative real part (in the left-half plane of the complex plane). In the frequency-domain framework and for closed-loop systems, the graphical Nyquist stability criterion is used. A closed-loop system (Fig. 2.4) is stable if and only if its open-loop frequency response  $\beta(j\omega)$  encircles (counter-clockwise) the  $(-1,0)$  critical point as many times as there are right-half plane poles in  $\beta(s)$ .

More than the stability property, it is interesting to analyze and then to ensure the stability degree of a closed-loop system. Several measures of the stability degree exist. They can be obtained both from the open-loop transfer function and from closed-loop transfer functions.

#### 2.3.1.1 Stability Margins from the Open-Loop Transfer Function

Four stability margins can be defined:

- the phase margin;
- the gain margin;
- the time-delay margin;
- the modulus margin.

**Fig. 2.4** Closed-loop system and its open-loop transfer function  $\beta(s)$

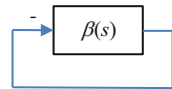


**Fig. 2.5** Open-loop transfer function  $\beta(s)$  feedbacked by a multiplicative uncertainty  $\Delta(s)$

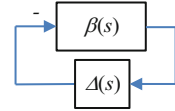
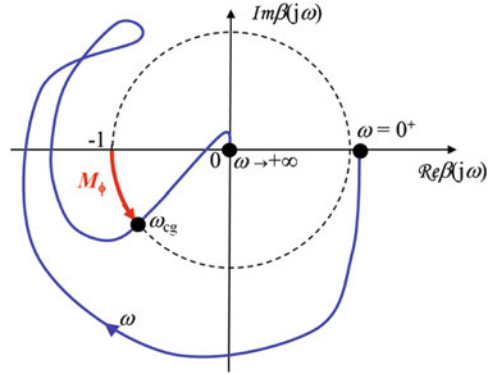


**Fig. 2.6** Definition of the phase margin



They indicate the smallest modifications of the open-loop that could make the stable closed-loop system unstable.

For a stable closed-loop system, the phase margin  $M_\Phi$  is the lowest phase variation of a pure-lag uncertainty block  $\Delta(s)$  (Fig. 2.5) that would make the closed-loop system unstable:

$$\Delta(j\omega_{cg}) \beta(j\omega_{cg}) = -1 \text{ with } \Delta(j\omega_{cg}) = e^{-jM_\Phi}. \quad (2.24)$$

The phase margin (Fig. 2.6) is measured at the open-loop gain crossover frequency and if  $-\pi$  is chosen for the argument of  $-1$ , it equals:

$$M_\Phi = \pi + \arg \beta(j\omega_{cg}). \quad (2.25)$$

For a stable closed-loop system, the gain margin  $M_G$  is the lowest gain variation of a pure-gain uncertainty block  $\Delta(s)$  (Fig. 2.5) that would make the closed-loop system unstable:

$$\Delta(j\omega_{cp}) \beta(j\omega_{cp}) = -1 \text{ with } \Delta(j\omega) = M_G. \quad (2.26)$$

The gain margin (Fig. 2.7) is measured at the open-loop phase crossover frequency  $\omega_{cp}$  (with  $\arg \beta(j\omega_{cp}) = -\pi$ ) and equals:

$$M_G = \frac{1}{|\beta(j\omega_{cp})|}. \quad (2.27)$$



**Fig. 2.7** Definition of the gain margin

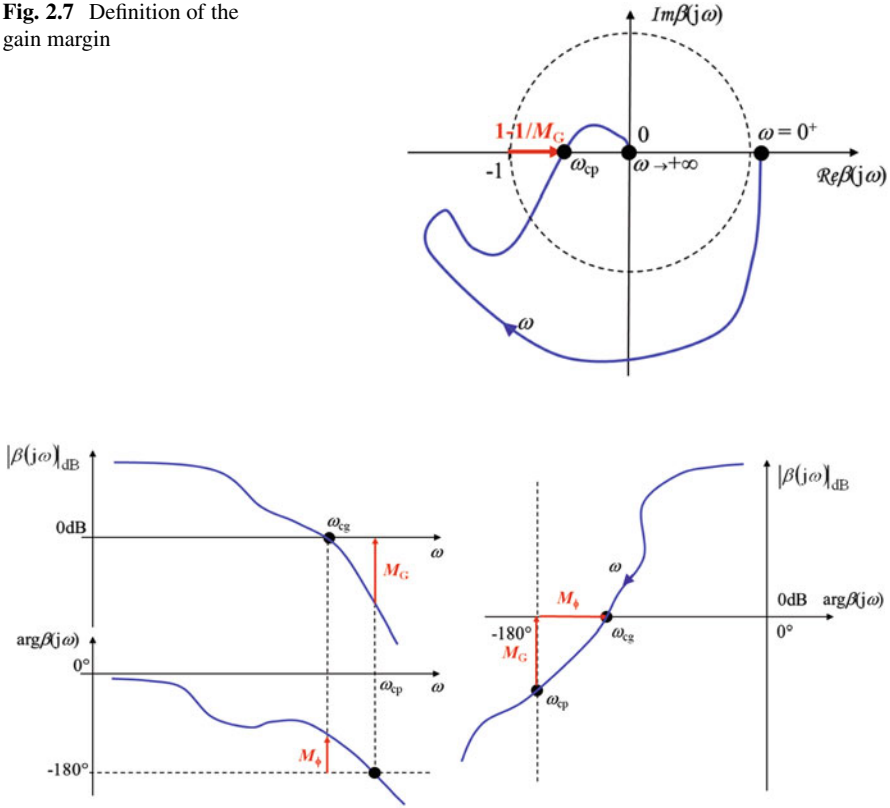


**Fig. 2.8** Measure of the phase and gain margins using a Bode diagram (*left*) or the Nichols plot (*right*) of  $\beta(j\omega)$

The gain and phase margins can be measured using the Bode diagram of the open-loop frequency response (Fig. 2.8).

For a stable closed-loop system, the time-delay margin  $M_{td}$  is the lowest value of a time-delay defining the uncertainty block  $\Delta(s)$  (Fig. 2.5) that would make the closed-loop system unstable:

$$\Delta(j\omega_{cg}) \beta(j\omega_{cg}) = -1 \text{ with } \Delta(j\omega_{cg}) = e^{-jM_{td}\omega_{cg}}. \quad (2.28)$$

If several open-loop gain crossover frequencies  $\omega_{cg}$  exist (Fig. 2.9), the time-delay margin equals:

$$M_{td} = \min_{\omega_{cg}} \left[ \frac{\pi + \arg \beta(j\omega_{cg})}{\omega_{cg}} \right]. \quad (2.29)$$

**Fig. 2.9** Definition of the time-delay margin

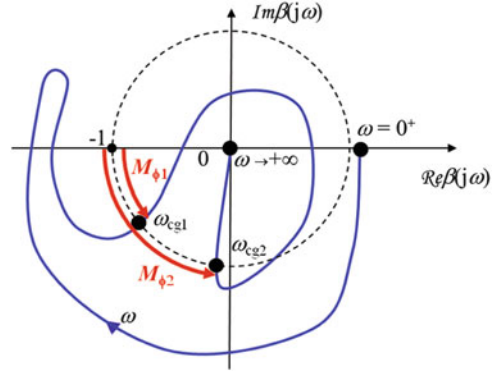


**Fig. 2.10** Open-loop transfer function  $\beta(s)$  and an additive uncertainty  $\Delta(s)$

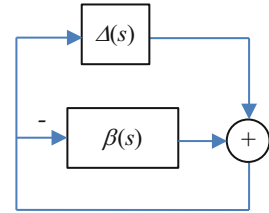
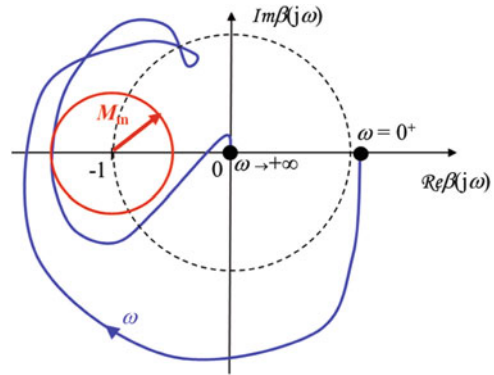


**Fig. 2.11** Definition of the modulus margin



For a stable closed-loop system, the modulus margin  $M_m$  is the lowest modulus of the uncertainty block  $\Delta(s)$  (Fig. 2.10) that would make the closed-loop system unstable:

$$\Delta(j\omega) + \beta(j\omega) = -1 \text{ with } \Delta(j\omega) = M_m e^{j\theta} \text{ and } -\pi \leq \theta \leq \pi. \quad (2.30)$$

As Fig. 2.11 shows, the modulus margin is the minimal distance between the open-loop frequency response and the  $-1$  critical point.

Thus, the modulus margin equals:

$$M_m = \min_{\omega} |1 + \beta(j\omega)|. \quad (2.31)$$

### 2.3.1.2 Stability Margins from Closed-Loop Transfer Functions

The closed-loop stability degree can also be estimated directly from time-domain closed-loop features:

- percentage overshoot  $O\%$  of the step response;
- damping ratio  $\zeta$  related to the dominant closed-loop pole pair if it exists.

Even if the stability margins defined from the open-loop frequency response are not always sufficient to predict and tune these time-domain features, the closed-loop stability degree can also be estimated directly from frequency-domain closed-loop features:

- the resonant peak  $M_r$  of the complementary sensitivity function  $|T(j\omega)|$  which is highly correlated to the percentage overshoot  $O\%$ ;
- the peak value of the sensitivity function  $|S(j\omega)|$ .

As Fig. 2.12 shows, from the open-loop frequency response,  $M_r$  can be determined (or set) using the magnitude contours of the Nichols chart.

It is not easy to determine the closed-loop damping ratio from an open-loop frequency response. In the same way that the Nichols chart was built to determine the resonant peak from the open-loop response, a set of iso-damping contours was built by using complex order fractional integration (Lanusse 1994; Lanusse et al. 2010, 2012; Oustaloup 1995; Oustaloup et al. 1995, 2003; Pommier-Budinger et al. 2008). In contrast, the peak value of the sensitivity function  $|S(j\omega)|$  does not accurately indicate any time-domain feature of the closed-loop system. If a modulus margin is required, it is interesting to note that:

$$\max_{\omega} |S(j\omega)| = \frac{1}{\min_{\omega} |1 + \beta(j\omega)|} = \frac{1}{M_m}. \quad (2.32)$$

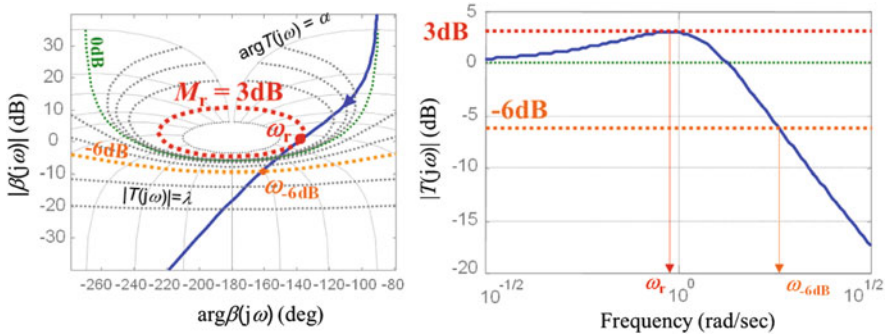


**Fig. 2.12** Open-loop frequency response and Nichols chart used to predict the closed-loop frequency response magnitude resonance peak

### 2.3.2 Uncertainty and Robustness

As the plant is perturbed and/or its model is uncertain, let a SISO perturbed plant be defined by

$$G(s) = G_{\text{nom}}(s)\Delta G(s), \quad (2.33)$$

where  $\Delta G(s)$  models a multiplicative uncertainty. The frequency uncertainty domains associated to the Nichols plot  $G_{\text{nom}}(j\omega)$  are defined by all the possible values of the pair  $\{|\Delta G(j\omega)|_{\text{dB}}, \arg \Delta G(j\omega)\}$ .

#### ■ Example 2.1

Let a perturbed plant  $G$  be defined by:

$$G(s) = \frac{k}{s(1 + \tau s)}, \quad (2.34)$$

with  $1 \leq k \leq 9$ ,  $0.1 \leq \tau \leq 10$ ,  $k_{\text{nom}} = 3$  and  $t_{\text{nom}} = 1$ .

Figure 2.13 shows the parametric uncertainty domain and the frequency uncertainty domain for  $\omega = 1 \text{ rad/s}$ .

21 values and a logarithmically spaced distribution were used for each plant parameter. Figure 2.13 shows that this permits a good definition of the uncertain frequency response of  $G$ . The red points locate the nominal parametrical state of the plant and the nominal frequency response of  $G(j\omega)$ . The green curve is the convex hull that contains all the possible values of  $G(j\omega)$  for  $\omega = 1 \text{ rad/s}$ . This convex hull can be used to define the frequency uncertainty domain  $D_1$  of  $G(j\omega)$  for  $\omega = 1 \text{ rad/s}$ . Figure 2.14 presents the frequency response of  $G(j\omega)$  for 140 frequencies logarithmically spaced between  $10^{-4} \text{ rad/s}$  and  $10^3 \text{ rad/s}$ .  $\square$

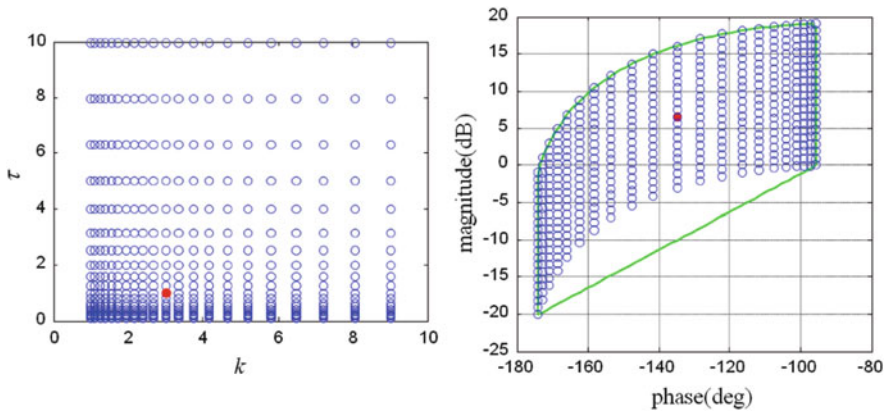


**Fig. 2.13** Variation of the plant parameters (*left*) and uncertain frequency response of  $G(j\omega)$  (*right*)

**Fig. 2.14** Nominal frequency response (*red*) of the plant and frequency uncertainty domains (*green*) in the Nichols chart

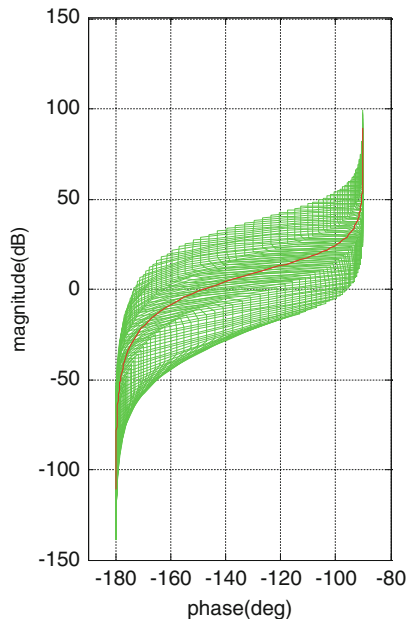
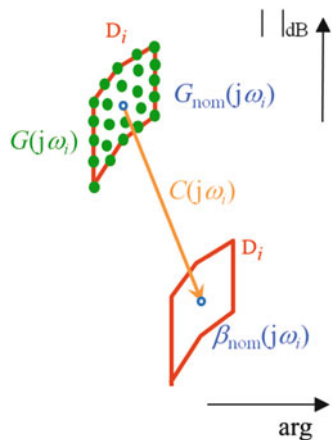


**Fig. 2.15** Constancy of frequency uncertainty domains in the Nichols chart

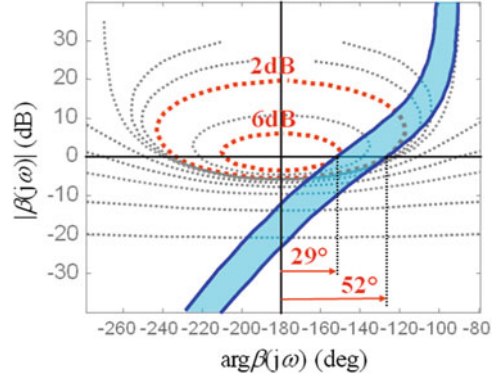


Taking into account a perturbed plant defined by (2.33) and a controller  $C(s)$ , the perturbed open-loop transfer function is defined by:

$$\beta(s) = G(s)C(s) = G_{\text{nom}}(s)\Delta G(s)C(s) = \beta_{\text{nom}}(s)\Delta G(s). \quad (2.35)$$

Thus, the frequency uncertainty domains associated to the Nichols plot of  $\beta_{\text{nom}}(j\omega)$  are also defined by the possible values of the pair  $\{|\Delta G(j\omega)|_{\text{dB}}, \arg \Delta G(j\omega)\}$ . Figure 2.15 shows that the nominal open-loop frequency response (that can be tuned

**Fig. 2.16** Open-loop frequency response resulting from a non-robust controller



thanks to the controller) can only move the frequency uncertainty domains  $D$  (in the Nichols chart) through longitudinal and vertical translations. They cannot be modified either in shape or in size.

Even if the final goal is the robustness of time-domain characteristics (overshoot  $O\%$  and/or damping ratio  $\zeta$ ), during a frequency-domain control system design, the stability degree robustness can be ensured by minimizing the variation in the phase margin  $M_\phi$ , or, more reliably, in the resonant peak  $M_r$ .

Figure 2.16 presents an open-loop frequency response whose frequency-response uncertainty comes from a perturbed plant. The designed controller is not robust as the phase margin  $M_\phi$  can vary from  $29^\circ$  to  $52^\circ$  and the resonant peak  $M_r$  from 2 dB to 6 dB. The goal of a robust controller is to minimize these variations as much as possible.

## 2.4 Frequency-Domain Design of PID Controllers

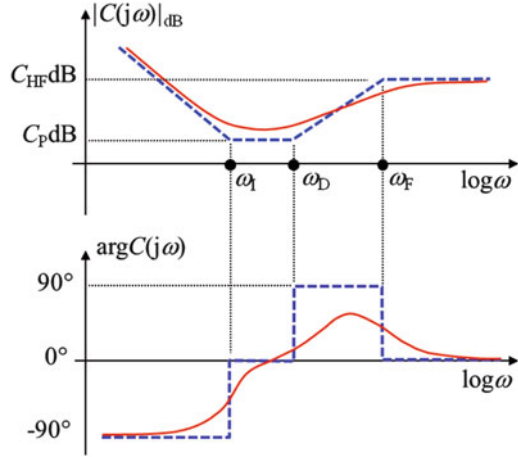
The *Proportional, Integral and Derivative* (PID) controller is widely used in industrial applications. It ensures speed, accuracy and stability degree performance. A parallel form of the PID controller is also often used. However, when an output feedback is used, a series form of the PID controller should be selected as it is easier to design.

### 2.4.1 Parallel PID Controller

The academic parallel PID is often defined by

$$C(s) = C_P + \frac{C_I}{s} + C_D s, \quad (2.36)$$

**Fig. 2.17** Frequency response of a parallel PID controller



where the three design parameters  $C_P$ ,  $C_I$  and  $C_D$  are the proportional, integral and derivative gains. As  $C(s)$  of (2.36) is improper, this definition needs to be modified to filter the derivative term with a  $\tau_f$  time constant:

$$C(s) = C_P + \frac{C_I}{s} + \frac{C_D s}{1 + \tau_f s}. \quad (2.37)$$

Figure 2.17 presents the Bode diagram of  $C(s)$ . For non-derivative plants, at low frequencies it shows that the integral term permits that:

- $T$  tends to 1 (2.7);
- $S$  tends to 0 (2.10);
- $SG$  tends to 0 (2.12).

For low-pass plants, at high frequencies the filtering term ensures that:

- $T$  tends to 0 (2.8);
- $CS$  tends to 0 (2.14).

Using (2.17), the proportional parameter  $C_P$  (but also the other two parameters) is generally chosen to set the open-loop gain cross-over frequency within the frequency range  $[\omega_D, \omega_F]$  with:

$$\omega_D = \frac{C_P}{C_D + C_P \tau_f} \text{ and } \omega_F = \frac{1}{\tau_f}. \quad (2.38)$$

The integral frequency  $\omega_I$  is:

$$\omega_I = \frac{C_I}{C_P}. \quad (2.39)$$

The high frequency gain of  $C(j\omega)$  is:

$$\lim_{\omega \rightarrow \infty} |C(j\omega)| = \frac{C_D + C_P \tau_F}{\tau_F}. \quad (2.40)$$

As (2.14) states that this gain is the high frequency gain of the control sensitivity function, thus the 3 design parameters must make it possible to meet a control effort constraint. These 3 parameters must also ensure a desired stability degree, for instance the phase margin defined by (2.25). Since each parameter acts on all requirements, a straightforward tuning of this parallel controller is more complex than tuning a series PID controller.

### 2.4.2 Series PID Controller

An easy-to-tune and series-improved PID can be defined by:

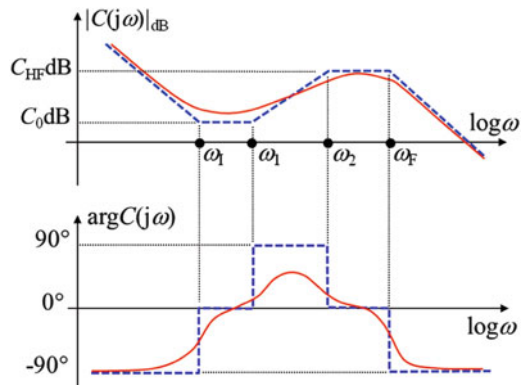
$$C(s) = C_0 \left(1 + \frac{\omega_I}{s}\right) \left(\frac{1 + s/\omega_1}{1 + s/\omega_2}\right)^{N_D} \frac{1}{1 + s/\omega_F}, \quad (2.41)$$

each term being band-limited and ensuring one of the controller behaviors: proportional, integral, derivative and filtering. The integer power  $N_D$  is used to permit both a large derivative action and the reduction in the high-frequency gain of the controller. The low-pass filter has been added to make the controller strictly proper and thus to decrease the gain of the control sensitivity function. Figure 2.18 presents the Bode diagram of  $C(s)$ .

The controller behavior is that of:

- an integrator for  $\omega \in ]0, \omega_I]$ ;
- a proportional gain for  $\omega \in [\omega_I, \omega_1]$ ;

**Fig. 2.18** Frequency response of a series PID(F) controller for  $N_D = 1$





- a differentiator for  $\omega \in [\omega_1, \omega_2]$ ;
- an amplifier for  $\omega \in [\omega_2, \omega_F]$ ;
- a low-pass filter for  $\omega \in [\omega_F, \infty[$ .

The high-frequency gain of  $C(j\omega)$  is bounded by:

$$|C(j\omega)|_{\omega \gg \omega_{cg}} < C_0 \left( \frac{\omega_2}{\omega_1} \right)^{N_D}. \quad (2.42)$$

Taking into account requirements such as a phase margin  $M_\Phi$  and an open-loop gain crossover frequency  $\omega_{cg}$ , the 5 parameters of this controller can be tuned with a straightforward methodology.

For  $\frac{\omega_{cg}}{\omega_1} = \frac{\omega_F}{\omega_{cg}}$ , the phase of the controller is

$$\arg C(j\omega_{cg}) = \Phi_M - 2 \arctan \frac{\omega_{cg}}{\omega_F}, \quad (2.43)$$

where  $\Phi_M$  is the lead or lag phase provided by the derivative term of the controller. For the phase margin requirement, it should be:

$$\Phi_M = -\pi + M_\Phi - \arg G(j\omega_{cg}) + 2 \arctan \frac{\omega_{cg}}{\omega_F}. \quad (2.44)$$

The ratio between  $\omega_{cg}$  and  $\omega_1$  (or between  $\omega_F$  and  $\omega_{cg}$ ) should be chosen as close as possible to one in order to provide high performance of the integral and filter behaviors. In contrast, such a small ratio could lead to too large a phase lead  $\Phi_M$  which would slow down the rejection of the input disturbance (decrease in the magnitude of the controller gain for frequencies lower than  $\omega_{cg}$ ) and would amplify even further the measurement noise (increase in the magnitude of the controller gain for frequencies greater than  $\omega_{cg}$ ). The difference between the plant phase  $\arg G(j\omega_{cg})$  and  $-\pi + M_\Phi$  is used to manage this tradeoff. The integer power  $N_D$  can be chosen greater than the number of radians in  $\Phi_M$  (1 rad is about  $57^\circ$ ).

For  $\frac{\omega_{cg}}{\omega_1} = \frac{\omega_2}{\omega_{cg}}$ , (2.42) is ensured if:

$$\frac{\omega_2}{\omega_{cg}} = \tan \frac{\frac{\Phi_M}{N_D} + \frac{\pi}{2}}{2} \text{ or } \frac{\omega_2}{\omega_{cg}} = \sqrt{\frac{1 + \sin\left(\frac{\Phi_M}{N_D}\right)}{1 - \sin\left(\frac{\Phi_M}{N_D}\right)}}. \quad (2.45)$$

Finally, from (2.17) the gain crossover frequency  $\omega_{cg}$  is ensured by:

$$C_0 = \frac{1}{\left( \frac{\omega_2}{\omega_{cg}} \right)^{N_D} |G(j\omega_{cg})|}. \quad (2.46)$$

The high-frequency gain (2.42) of the controller needs to be computed to verify if the high-frequency control sensitivity function gain is not too large. If it is,  $\omega_{cg}$

should be reduced and all the parameters recomputed. A good way to estimate an initial value of  $\omega_{cg}$  is to use (2.18) and (2.42). For a positive  $N_D$  (controller with a derivative action),

$$|C(j\omega)|_{\omega > \omega_{cg}} = \frac{1}{|G(j\omega_{cg})|} \left( \frac{\omega_2}{\omega_1} \right)^{\frac{N_D}{2}}. \quad (2.47)$$

Thus, constraint (2.19) is now replaced by:

$$|G(j\omega_{cg})| \geq \left( \frac{\omega_2}{\omega_1} \right)^{\frac{N_D}{2}} \frac{0.1 |n_m|}{u_{SAT}}, \quad (2.48)$$

where  $(\omega_2/\omega_1)^{N_D/2}$  is a factor as large as the phase lead needs to be. This factor can be set to 4 or more when the exact phase lead required is unknown.

### ■ Example 2.2

Let a plant  $G$  be defined by:

$$G(s) = \frac{k}{s(1+\tau s)} \text{ with } k_{nom} = 10 \text{ and } \tau_{nom} = 1,000s. \quad (2.49)$$

A PID controller is tuned for the nominal values of  $k$  and  $\tau$ . The requirements are:

- limitation of the control effort  $u$  due to the high-frequency measurement noise  $n_m$  (need for a low-pass filter);
- reduction in the steady-state effect of a step input disturbance  $d_u$  to zero with a settling time as short as possible (need for an integral action);
- a step response of  $y$  to a reference input  $y_{ref}$  with a percentage overshoot around 30 % and a settling time as short as possible.

Let us consider that the control effort limitation permits a rise time of about 0.2 s and thus using (2.48) a value of  $\omega_{cg}$  of about 5 rad/s. A phase margin of  $50^\circ$  would lead to an overshoot of about 30 %.

For  $\omega_{cg} = 5$  rad/s, the magnitude and phase of the plant are  $|G(j5)| = 4.10^{-4}$  and  $\arg G(j5) \approx -180^\circ$ . To avoid too large a value of  $\Phi_M$ , the integral and filter actions are tuned with  $\frac{\omega_{cg}}{\omega_1} = \frac{\omega_F}{\omega_{cg}} = 10$ . Using (2.44),  $\Phi_M = 61.4^\circ$  and  $N_D = 2$ . From (2.45),  $\frac{\omega_2}{\omega_{cg}} = 1.76$  and from (2.46)  $C_0 = 833$ . Thus the controller is:

$$C(s) = 833 \left( 1 + \frac{0.5}{s} \right) \left( \frac{1 + s/2.84}{1 + s/8.8} \right)^2 \frac{1}{1 + s/50}. \quad (2.50)$$

From (2.42), its high frequency gain is lower than 7,750.

Even if the PID controller has been tuned for a nominal plant, it is now assessed for 3 values of  $\tau$ :  $\tau = \tau_{nom}/3$ ,  $\tau = \tau_{nom}$  and  $\tau = \tau_{nom} * 3$ . For the 3 parametric states of the plant, Figs. 2.19, 2.20 and 2.21 present respectively the open-loop Nichols plot, the closed-loop sensitivity functions and the step responses.

**Fig. 2.19** Open-loop Nichols plot for the 3 values of  $\tau$ :  $\tau = \tau_{\text{nom}}/3$  (---),  $\tau = \tau_{\text{nom}}$  (—) and  $\tau = \tau_{\text{nom}}*3$  (---)

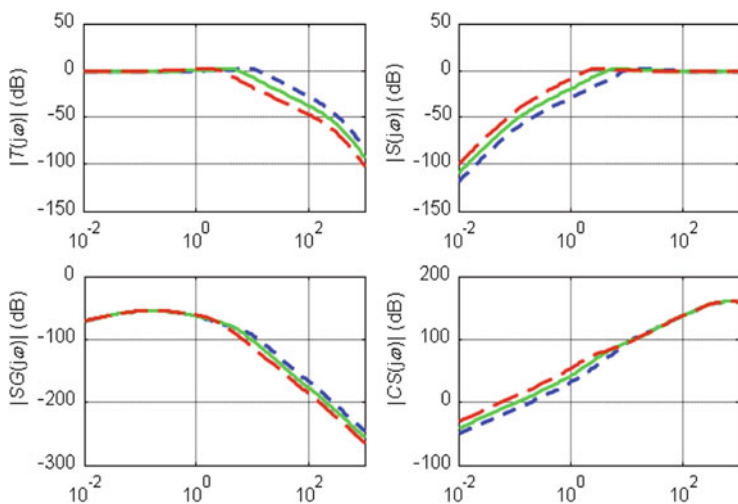
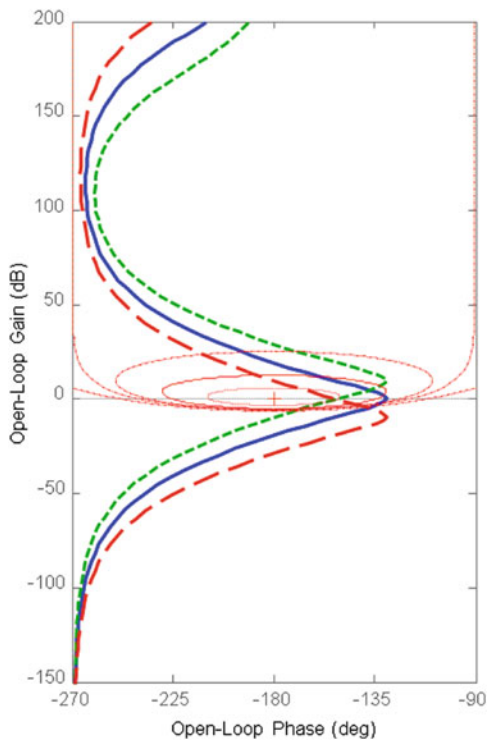


**Fig. 2.20** Closed-loop sensitivity functions for the 3 values of  $\tau$ :  $\tau = \tau_{\text{nom}}/3$  (---),  $\tau = \tau_{\text{nom}}$  (—) and  $\tau = \tau_{\text{nom}}*3$  (---)

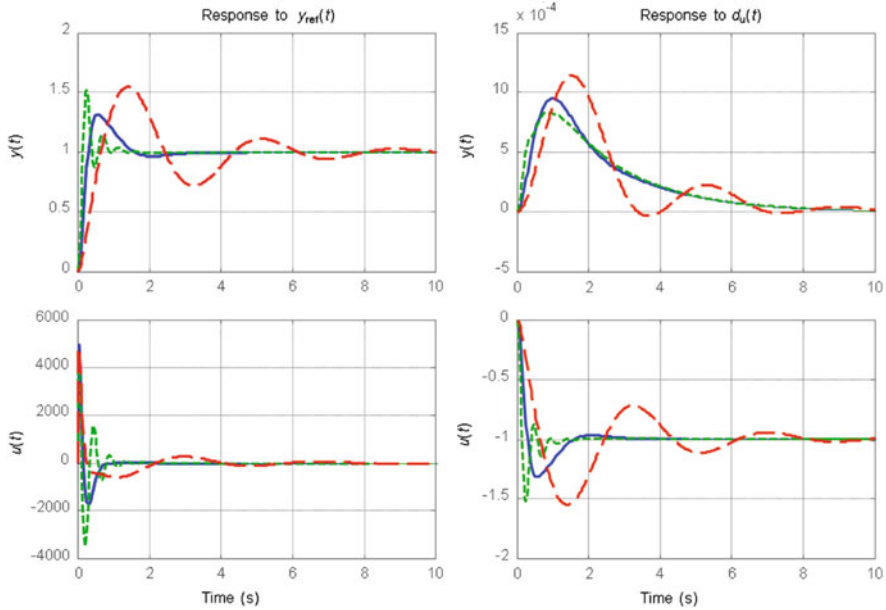


**Fig. 2.21** Closed-loop step responses for the 3 values of  $\tau$ :  $\tau = \tau_{\text{nom}}/3$  (---),  $\tau = \tau_{\text{nom}}$  (—) and  $\tau = \tau_{\text{nom}}*3$  (---)

When  $\tau$  is perturbed, Fig. 2.19 shows that the phase and gain margin can be no more than  $28^\circ$  and 9.7 dB. Furthermore the Nichols chart magnitude contours indicate that the resonance peak of  $T$  can increase significantly. Figure 2.20 shows that:

- $T$  is close to 0 dB (accurate tracking of the reference signal) and  $S$  small (good desensitization) up to 1 rad/s;
- $SG$  decreases (efficient rejection of input disturbance) when  $\omega$  decreases from 1 rd/s;
- $CS$  reaches about 80 dB at 10 rd/s and then decreases (low amplification of noise measurement);
- even if the nominal resonant peak of  $T$  is 3.2 dB, it reaches 8.1 dB for  $\tau = 3*\tau_{\text{nom}}$ ;
- even if the nominal resonant peak of  $S$  is 3.27 dB (modulus margin about 0.69), it reaches 8 dB (modulus margin about 0.40) for  $\tau = \tau_{\text{nom}}/3$ .

Figure 2.21 shows that:

- for long durations, the tracking of  $y_{\text{ref}}$  and the rejection of  $d_u$  are efficient;
- even if the nominal percentage overshoot for the response of  $y$  to  $y_{\text{ref}}$  is 31 %, it reaches 53 % for  $\tau = \tau_{\text{nom}}*3$ ;

- the response of  $u$  to  $y_{\text{ref}}$  quickly reaches 5,000 (2 times lower than the predicted level given by  $10^{80/20}$ );
- the responses of  $y$  to  $y_{\text{ref}}$  and to  $d_u$  are too lightly damped when  $\tau$  is perturbed.

To sum up, it shows that a PID controller (well) tuned for a nominal plant is not robust when the plant is perturbed.  $\square$

### 2.4.3 Design of a Digital Controller

When the controller has to be discrete-time implemented within a processor, it is usual to design it with a continuous time-domain methodology and then to discretize the derivative operator by using a small sampling time. Unfortunately, this leads both to a lengthy processing time and to a bad condition number of the resulting digital controller. To avoid these problems, the initial digital control system design problem with the sample period  $T_s$  can be transformed into a pseudo-continuous problem by:

- taking into account the transfer function of a zero-order hold on the plant input;
- computing the z-transform of the continuous-time set {plant and hold};
- achieving a bilinear variable change, for instance  $z^{-1} = (1 - w) / (1 + w)$ .

So,  $G(s)$  becomes successively  $G_0(s) = B_0(s)G(s)$ , where  $B_0(s)$  is the transfer function of the zero-order hold

$$B_0(s) = \frac{1 - e^{-sT_s}}{s}, \quad (2.51)$$

then  $G_0(z) = Z\{G_0(s)\}$  and finally  $G_0(w)$ .

The controller  $C(w)$  defined by

$$C(w) = C_0 \left(1 + \frac{v_1}{w}\right) \left(\frac{1 + w/v_1}{1 + w/v_2}\right)^{N_D} \frac{1}{1 + w/v_F}, \quad (2.52)$$

can be designed using a frequency-domain method knowing that  $G_0(w)$  (with  $w = j\nu$  and the normalized pseudo-frequency  $\nu = \tan(\omega T_s/2)$ ) is the exact frequency response of  $G_0(z)$  (with  $z = e^{j\omega T_s}$ ). The particular value  $\nu = 1$  is a high frequency as it is equivalent to  $\omega = \omega_s/4$  with  $\omega_s = 2\pi/T_s$ .  $\nu_{\text{cg}} = 0.2$  is generally the greatest value that can be used.

Finally, the digital controller  $C(z^{-1})$  is obtained by achieving the inverse variable change  $w = (1 - z^{-1})/(1 + z^{-1})$  of  $C(w)$ .

#### ■ Example 2.3

A digital controller with  $T_s = 50$  ms is designed for  $G$  defined by Example 2.2. It has to ensure  $M_\Phi = 50^\circ$  and  $\omega_{\text{cg}} = 5$  rad/s.

The z-transform of  $G(s)$  plus a zero-order hold is:

$$G_0(z^{-1}) = Z\{B_0(s)G(s)\} = \frac{1.25 * 10^{-5} z^{-1} (1 + z^{-1})}{1 - 2z^{-1} + z^{-2}}. \quad (2.53)$$

The pseudo continuous-time transfer function of  $G_0$  is:

$$G_0(w) = \frac{5.208 * 10^{-11} w - 6.25 * 10^{-6} w + 6.25 * 10^{-6}}{w^2 + 2.5 * 10^{-5} w + 1.872 * 10^{-18}}. \quad (2.54)$$

The pseudo-frequency is  $v_{cg} = 0.1257$ . The w-transfer function of the PID controller is:

$$C(w) = \frac{3.195w^3 + 0.4645w^2 + 0.01942w + 1.771 * 10^{-4}}{(2.834w^3 + 4.908w^2 + 1.853w + 0.2013) * 10^{-4} w}. \quad (2.55)$$

Finally the digital controller  $C(z^{-1})$  is:

$$C(z^{-1}) = \frac{-2807z^{-4} + 6484z^{-3} - 947z^{-2} - 6483z^{-1} + 3756}{-0.04312z^{-4} - 0.1961z^{-3} + 1.357z^{-2} - 2.118z^{-1} + 1}. \quad (2.56)$$

Figure 2.22 compares the step response of the plant with this digital controller to the step response obtained with the continuous-time controller defined by (2.46). With or without the time discretization, the responses are very close. When the effect of the time discretization is well managed, it shows that a relatively large sampling time can be chosen versus the desired speed of  $y$ .  $\square$

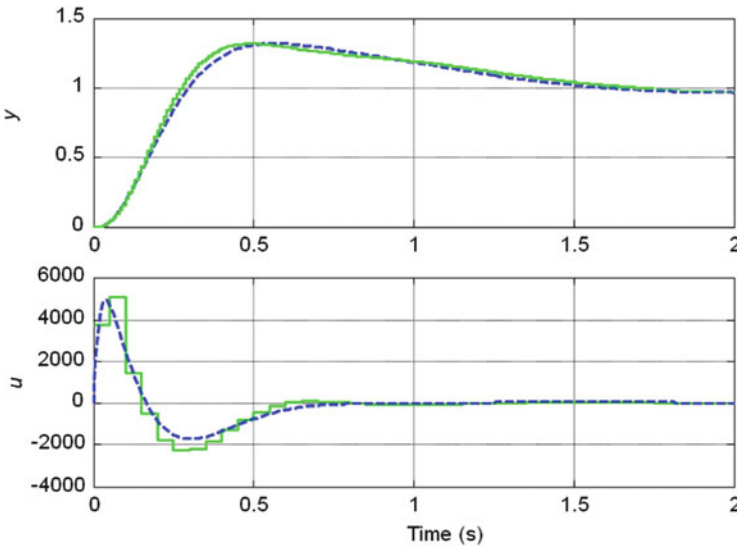


Fig. 2.22 Comparison of the closed-loop responses with a digital or continuous-time controller

### 2.4.4 Design of an Anti-windup System

While it is very useful to apply a plant input equal to its saturation levels to ensure short settling times, it is very important to be able to exit this saturation functioning mode rapidly. If this is not the case, a windup phenomenon can occur, making the closed-loop system unstable. As the windup problem often comes from an integrating behavior of the plant input, a very simple and continuous-time solution is presented by Fig. 2.23. This anti-windup system is based on an inner loop that feedbacks the integral part of the linear controller so that the controller output remains close to the saturated levels during saturation times.

$C'(s)$  is defined from the initial linear controller  $C(s)$  as:

$$C(s) = C'(s) \left(1 + \frac{\omega_I}{s}\right). \quad (2.57)$$

Gain  $\alpha_I$  is such that the open-loop gain crossover frequency of the integral inner loop is about the integration frequency  $\omega_I$  ( $\alpha_I \approx 1$ ). Then the linear behavior of the new controller remains the same as before and the output  $u(t)$  tracks its saturated value  $u_{\text{SAT}}(t)$  provided by the model of the plant input saturation.

#### ■ Example 2.4

Using the same example as before (Example 2.2), the transfer function of the controller previously designed by (2.50) can be written:

$$C(s) = C'(s) \left(1 + \frac{0.5}{s}\right) \text{ with } C'(s) = 833 \left(\frac{1+s/2.84}{1+s/8.8}\right)^2 \frac{1}{1+s/50}. \quad (2.58)$$

The absolute value of the plant input is assumed to be 5,000. For a 50-step variation in the reference signal  $y_{\text{ref}}(t)$ , Fig. 2.24 compares the input  $u_{\text{sat}}(t)$  and the output  $y(t)$  of  $G(s)$  obtained with or without the anti-windup system of Fig. 2.23 (tuned with  $\alpha_I = 1$ ). As it limits the overshoot of the output, this anti-windup system proves its ability to manage the saturation effect on the plant input.  $\square$

Following several anti-windup propositions (Wurmthaler and Hippe 1991; Ygorra et al. 1996; Goodwin et al. 2001), Fig. 2.25 presents a generalization of

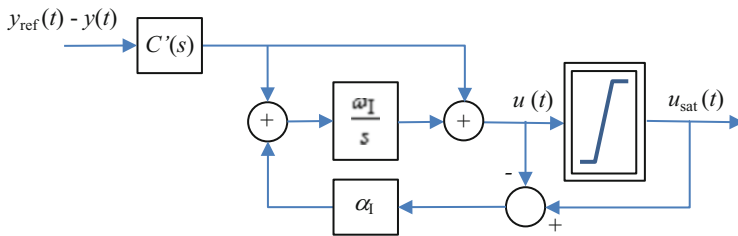
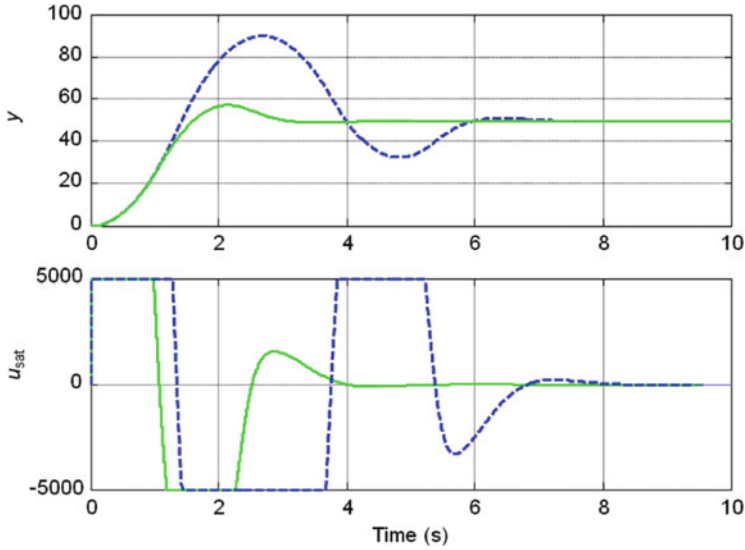
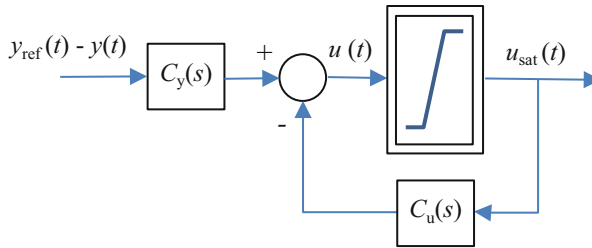


Fig. 2.23 Anti-windup system



**Fig. 2.24** Comparison of the closed-loop responses with (solid line) or without (dashed line) the anti-windup system of Fig. 2.22



**Fig. 2.25** Generalization of the anti-windup solution

this anti-windup solution where the initial controller has been split so that the linear behavior of the new controller remains the same as before, that is to say:

$$C(s) = \frac{C_y(s)}{1 + C_u(s)}. \quad (2.59)$$

The anti-windup systems of Fig. 2.23 and 2.25 behave exactly the same if:

$$C_y(s) = C'(s) \frac{1 + \frac{p}{\omega_I}}{\alpha_I + \frac{p}{\omega_I}} \quad (2.60)$$

and

$$C_u(s) = -\frac{\alpha_I}{\alpha_I + \frac{p}{\omega_I}}. \quad (2.61)$$



Presenting the closed-loop system as a Lure's system (Popov 1962),  $C_u(s)$  and  $C_y(s)$  can also be designed by using a methodology that avoids the Nyquist or Nichols plot of the linear system  $L(s) = C_u(s) + C_y(s)G(s)$  crossing the locus of the (opposite and inverse of the) saturation nonlinearity describing function  $N(u_1)$  (Krylov and Bogoliubov 1943; Kochenburger 1950). Thus, this approach takes into account both the linear model of the plant and of the controller. It has been extended to fractional order controllers in (Lanusse and Oustaloup 2005; Lanusse et al. 2007).

### ■ Example 2.5

Using the same example as before and the describing function approach, the same linear behavior to that of  $C(s)$  defined by (2.50) can be ensured by using:

$$C_u(s) = -\frac{0.4375s + 0.0625}{s^2 + 0.5s + 0.0625} \quad (2.62)$$

and

$$C_y(s) = 10^5 \frac{3.999s^4 + 24.96s^3 + 45.16s^2 + 18.85s + 1.008}{s^5 + 68.1s^4 + 991.3s^3 + 4355s^2 + 1996s + 242}, \quad (2.63)$$

which avoids  $C_u(j\omega) + C_y(j\omega)G(j\omega)$  crossing  $-1/N(u_1)$  defined from

$$\begin{cases} N(u_1) = \frac{2}{\pi} \left\{ \arcsin \frac{5000}{u_1} + \frac{5000}{u_1} \sqrt{1 - \frac{5000^2}{u_1^2}} \right\} \text{ pour } u_1 \geq 5000 \\ N(u_1) = 1 \text{ for } u_1 \leq 5000 \end{cases} \quad (2.64)$$

For a 50-step variation in the reference signal  $y_{\text{ref}}(t)$ , Fig. 2.26 compares the input  $u_{\text{sat}}(t)$  and the output  $y(t)$  of  $G(s)$  obtained with or without the anti-windup system of Fig. 2.24 where  $C_u(s)$  and  $C_y(s)$  are respectively defined by (2.62) and (2.63). As with the previous anti-windup solution, it shows that this anti-windup system is able to manage the saturation effect.  $\square$

## 2.5 Fractional Order PID Controllers

Fractional order derivatives and integrals can be used to generalize the well-known PID controller.

### 2.5.1 Parallel $PI^\lambda D^\mu$ Controller

Replacing the Laplace variable  $s$  by fractional powers of  $s$ , the parallel PID becomes a  $PI^\lambda D^\mu$  defined by:

$$C(s) = C_P + \frac{C_I}{s^\lambda} + C_D s^\mu \text{ with } (\lambda, \mu) \in \mathbb{R}^2. \quad (2.65)$$

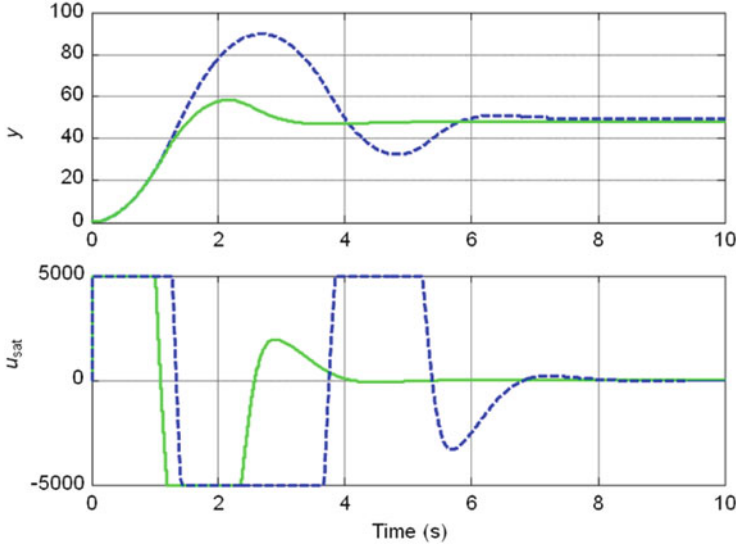


**Fig. 2.26** Comparison of the closed-loop responses with (solid line) or without (dashed line) the anti-windup system of Fig. 2.24

The interest of this controller is its greater flexibility (through two more design parameters  $\lambda$  and  $\mu$ ). Some studies (Tustin 1958; Manabe 1960; 1961; Petras 1999; Podlubny 1999; Chen et al. 2004; Monje et al. 2004, 2010; Cervera and Baños 2006; Nataraj and Tharewal 2010; Valerio and Sa da Costa 2012) dedicated to the class of fractional order PID controllers explain how to use this flexibility to solve control problems. Often, no integral or derivative part is used and only a  $PI^\lambda$  or  $PD^\mu$  is designed. As for the integer order PID controller, to avoid the CS sensitivity function tending to infinity, the fractional PID controller needs to be modified:

$$C(s) = C_P + \frac{C_I}{s^\lambda} + \frac{C_D s^\mu}{1 + \tau_F s^\gamma}. \quad (2.66)$$

Depending on the value of  $\gamma$ ,  $C(s)$  is biproper for  $\gamma = \mu$  and strictly proper for  $\gamma > \mu$ . Figure 2.27 shows a Bode diagram of  $C(s)$  for  $\gamma = \mu$ .

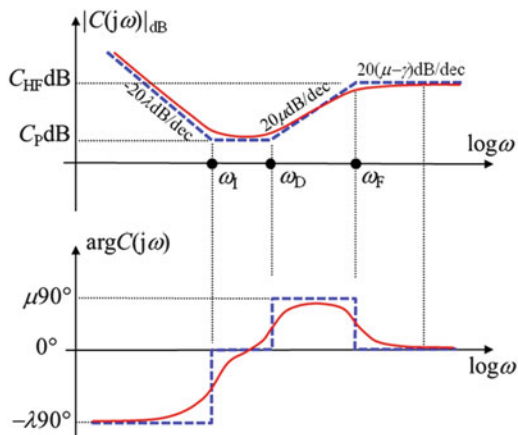
In Fig. 2.27, even if the high frequency gain of  $C(j\omega)$  remains defined as in the integer case by (2.40), the corner frequencies are now defined by:

$$\omega_I = \left( \frac{C_I}{C_P} \right)^{1/\lambda}, \quad \omega_D = \left( \frac{C_P}{C_D + C_P \tau_F} \right)^{1/\mu} \quad \text{and} \quad \omega_F = \left( \frac{1}{\tau_F} \right)^{1/\gamma}. \quad (2.67)$$

As five design parameters can be tuned, five (or more) different requirements can be taken into account. They can be chosen among:

- a given phase margin
- a given gain margin

**Fig. 2.27** Frequency response of a biproper  $PI^\lambda D^\mu$  controller ( $\gamma = \mu$ )



- a given open-loop gain crossover frequency  $\omega_{cg}$
- a flat open-loop phase around  $\omega_{cg}$  (for plants with gain perturbation)
- a given controller high-frequency gain
- no steady-state error
- given gains at given frequencies of the four closed-loop sensitivity functions.

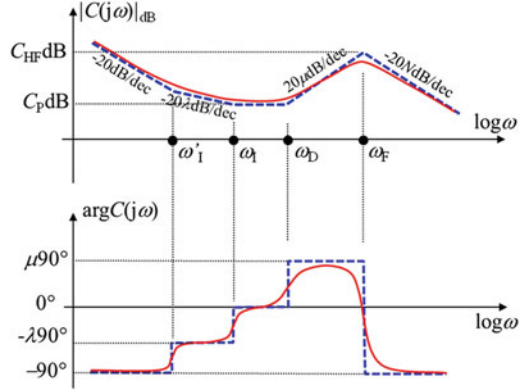
### 2.5.2 Academic Parallel $PI^\lambda D^\mu$ Controller Drawbacks

If the fractional PID controller (2.66) is used to solve a control problem, three major drawbacks can arise.

1. Although it is interesting to use a fractional differentiation transfer function for a lead effect and to shape the open-loop phase, the fractional integrator transfer function is of little interest since for an input disturbance of the form  $1/s^k$ , a fractional integrator of order  $\lambda = k + \alpha$  (with  $k \in \mathbb{N}$  and  $0 < \alpha < 1$ ) is no more efficient (or even less so) for steady-state error cancellation than a simpler integer integrator of order  $\lambda = k + 1$ .
2. It would require a highly resource-consuming discrete-time implementation of the fractional order  $\lambda$  integrator to avoid its band-limitation at low frequencies. Moreover, this mandatory band-limitation for the implementation leads to a controller that behaves like an integer integrator.
3. If  $\gamma$  differs from  $\mu$ , it would also require a highly resource-consuming discrete-time approximation or an infinite order equivalent continuous-time model to implement the high-frequency behavior of the order  $\mu$  derivative part.

Note that as their gains tend towards 0, respectively at high and low frequencies, even if the fractional order integrator and derivative operator are band-limited for the controller implementation, they can be achieved without modifying the global controller behavior.

**Fig. 2.28** Frequency response of a strictly proper  $PI^\lambda D^\mu$  controller with  $N = 1$



To avoid the third drawback, it is useful to choose  $\gamma$  such that  $\gamma - \mu = (N \in \mathbb{N})$  with  $N=0$  for a biproper controller or  $N>0$  for a strictly proper controller.

The first and second drawbacks can be avoided by replacing the fractional order integrator by a fractionally band-limited integer order (Maamri et al. 2010) that can be approximated with a low order rational transfer function. Thus, for  $0 < \lambda < 1$ , the fractional  $PI^\lambda D^\mu$  becomes

$$C(s) = C_P + C'_1 \frac{1 + \left(\frac{s}{\omega'_1}\right)^{1-\lambda}}{s} + \frac{C_D s^\mu}{1 + \tau_F s^{N+\mu}}, \quad (2.68)$$

where  $C'_1$  equals  $\omega'_1{}^{\lambda-1} C_1$  to ensure the same  $\omega_1$  corner frequency as in (2.65). Figure 2.28 depicts the Bode diagram of this modified parallel fractional controller.

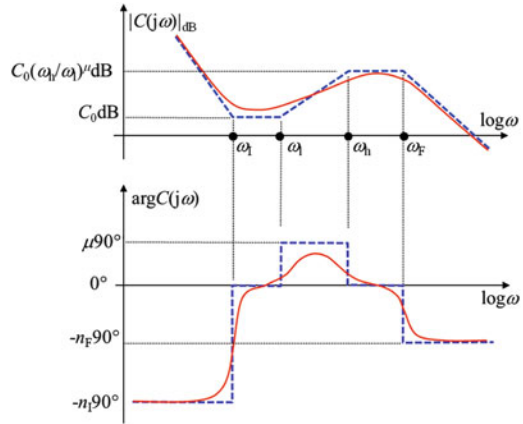
### 2.5.3 Series Fractional Order $PID^\mu$ Controller

In order to simplify its design and implementation, without loss of performance, it is possible to choose a fractional order  $PID^\mu$  controller defined by:

$$C(s) = C_0 \left(1 + \frac{\omega_l}{s}\right)^{n_l} \left(\frac{1 + \frac{s}{\omega_l}}{1 + \frac{s}{\omega_h}}\right)^\mu \frac{1}{\left(1 + \frac{s}{\omega_F}\right)^{n_F}}, \quad (2.69)$$

with  $\omega_l \leq \omega_1 \leq \omega_h \leq \omega_F$  and  $n_l \in \mathbb{N}$ ,  $\mu \in \mathbb{R}$ ,  $n_F \in \mathbb{N}$ . Figure 2.29 presents a Bode diagram of this  $PID^\mu(F)$  controller. The following algorithm can be used to tune the controller.

**Fig. 2.29** Frequency response of a series fractional order  $PID^\mu$  controller for:  $n_I = 2$ ,  $n_F = 1$  and  $\mu = 0.75$



1. Let us consider the control diagram of Fig. 2.1 in which, at low frequencies ( $\omega < \omega_l$ ), the reference input signal spectrum is defined by  $Y_{ref}(s) \approx y_{ref0}/s^M$  and the plant input disturbance spectrum is defined by  $D_u(s) \approx d_{u0}/s^N$ . If  $n_{pl}$  represents the integral order of the asymptotic behavior of the plant at low frequencies, order  $n_I$  of the proportional integrator is defined by  $n_I \geq \max(M - n_{pl}, N)$  to ensure no steady state error.
2. The low-pass filter order  $n_F$  is simply  $n_F \geq 0$ , given that (with increasing frequency and for  $\omega > \omega_F$ )  $n_F = 0$  ensures the constancy of the gain of the input sensitivity function  $CS(j\omega)$ , and  $n_F \geq 1$  ensures its decrease.
3. Choose an open-loop gain crossover frequency  $\omega_{cg}$  to reach the bandwidth specification.
4. Choose  $\omega_l = \omega_{cg}/\alpha_l$  with  $\alpha_l \in [1, 10]$  according to settling time specifications.
5. Choose  $\omega_F = \alpha_F \omega_{cg}$  with  $\alpha_F \in [1, 10]$  according to noise immunity requirements.
6. Compute  $\omega_l$ ,  $\omega_h$  and  $\mu$  to obtain the required phase margin  $M_\Phi$  and  $C_0$  to obtain the desired open-loop gain crossover frequency  $\omega_{cg}$ .

As four parameters ( $\omega_l$ ,  $\omega_h$ ,  $\mu$  and  $C_0$ ) are used to define two requirements ( $\omega_{cg}$  and  $M_\Phi$ ) only, up to two additional requirements can be taken into account.

### ■ Example 2.6

Let a plant (a DC motor) be defined by:

$$G(s) = \frac{\Omega(s)}{U(s)} = \frac{K_u}{(T_e s + 1)(J_m s + f)} \quad (2.70)$$

with  $K_u = 2.34 \text{ Nm/V}$ ,  $T_e = 0.043 \text{ s}$ ,  $J_m = 0.108 \text{ kg.m}^2$  and  $f = 0.002 \text{ Nm.s.rad}^{-1}$ .

The  $PID^\mu$  requirements are:

- $\omega_{cg} = 100 \text{ rad/s}$
- $M_\Phi = 50^\circ$

- a low-pass filtering with  $n_F = 1$  and  $\omega_F/\omega_{cg} = 5$
- an integration with  $n_I = 1$  and  $\omega_{cg}/\omega_1 = 5$ .

To facilitate the tuning of the controller, we choose  $\omega_{cg} = \sqrt{\omega_1\omega_2}$ . For  $\mu = 2$ , the design problem is that of the integer order PID defined by (2.41) and no more requirements can be taken into account. The phase margin and open-loop gain crossover frequency are ensured with  $N_D = 2$ ,  $\omega_{cg}/\omega_1 = \omega_2/\omega_{cg} = 1.742$  and  $C_0 = 6.858$ . Thus the controller is:

$$C(s) = 6.858 \left(1 + \frac{20}{s}\right) \left(\frac{1 + s/58.02}{1 + s/172.4}\right)^2 \frac{1}{1 + s/500}. \quad (2.71)$$

It provides a gain margin of 15.2 dB.

Using the fractional order PID $^\mu$  defined by (2.69) with  $\omega_{cg} = \sqrt{\omega_1\omega_2}$ , one more requirement can be taken into account. For instance, a 20 dB gain margin can be achieved with  $\mu = 0.815$ ,  $\omega_{cg}/\omega_1 = \omega_2/\omega_{cg} = 6.65$  and  $C_0 = 4.338$ . The controller is:

$$C(s) = 4.338 \left(1 + \frac{20}{s}\right) \left(\frac{1 + s/15.04}{1 + s/665}\right)^{0.815} \frac{1}{1 + s/500}. \quad (2.72)$$

Figure 2.30 shows how the fractional order controller can move the open-loop frequency response away from the critical point. Even if both controllers ensure the same open-loop gain crossover frequency and phase margin, Fig. 2.31 shows that this fractional order controller provides a phase lead over a greater frequency range,

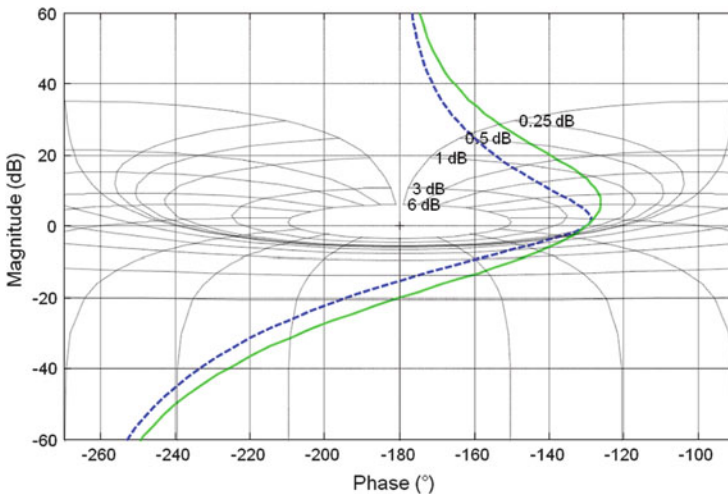


**Fig. 2.30** Comparison of the Nichols plot of the open-loop frequency responses obtained with the integer order (*dashed line*) and fractional order (*solid line*) controllers

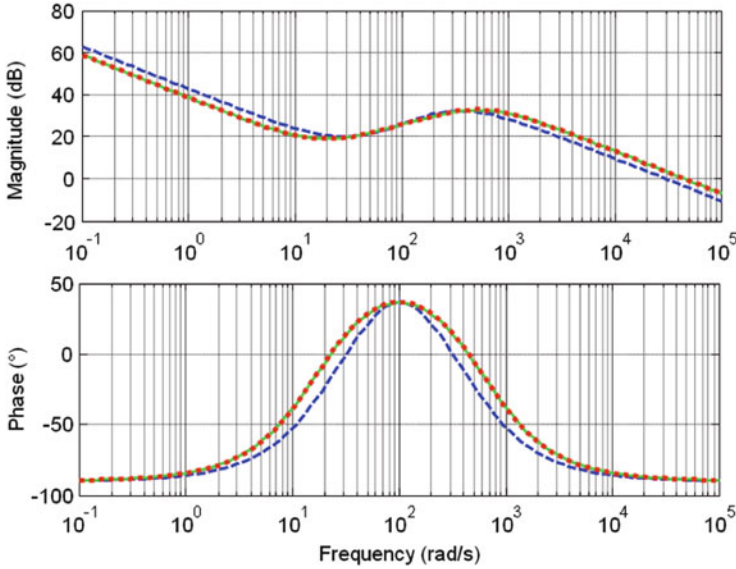


**Fig. 2.31** Comparison of the Bode diagram of the integer order controller (*dashed line*) and of the fractional order controller before (*solid line*) and after (*dotted line*) its approximation

which could be useful in a robustness framework. However, the fractional controller gives a lower gain at low frequencies and a greater gain at high frequencies, which could respectively increase the magnitude of the *SG* input sensitivity function and of the *CS* control sensitivity function.

In order to implement the fractional order controller, Oustaloup's approximation method (Oustaloup 1981) is used to replace its order 0.815 part by a rational one. As there are less than two decades between  $\omega_l$  and  $\omega_h$ , Fig. 2.31 shows that only three zero/pole pairs permit a good approximation of the fractional order transfer function. Then, the controller defined by (2.72) can be implemented using:

$$C(s) = 4.338 \left( 1 + \frac{20}{s} \right) \frac{1 + s/16.89}{1 + s/47.36} \frac{1 + s/54.71}{1 + s/167.5} \frac{1 + s/211.2}{1 + s/592.2} \frac{1}{1 + s/500}. \quad (2.73)$$

Figure 2.32 compares the magnitude of the four closed-loop sensitivity functions obtained with the integer order PID and with the fractional order one. They are very close even if slightly larger magnitudes of *SG* and *CS* can be detected for the fractional order controller. A lower rejection of input disturbance and a higher sensitivity of the control effort is the price to pay for a wider phase lead frequency range. Figure 2.33 shows that even if the step responses to  $y_{\text{ref}}(t)$  are close, the rejection of the input disturbance is slower for the fractional order controller than for the integer one.  $\square$

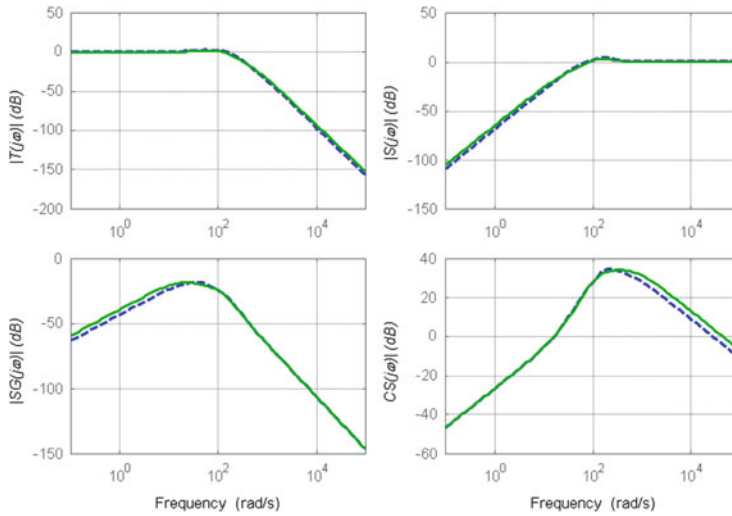


**Fig. 2.32** Closed-loop sensitivity functions for the integer order (*dashed line*) and fractional order (*solid line*) controllers

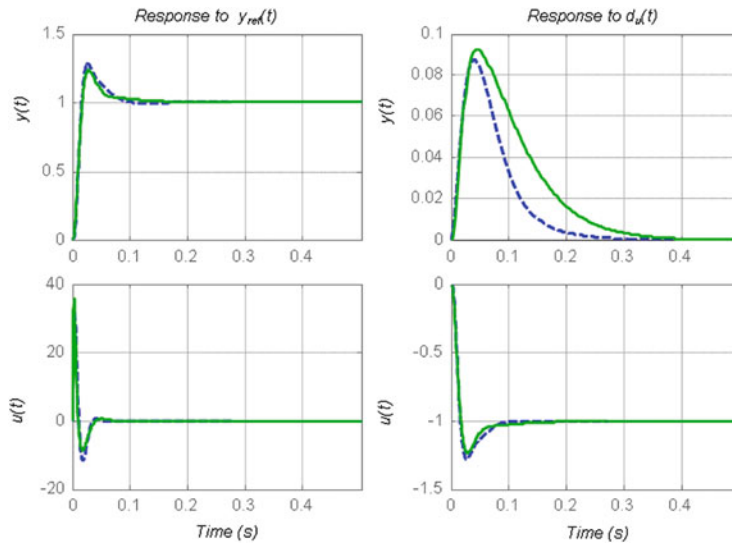


**Fig. 2.33** Closed-loop step response for the integer order (*dashed line*) and fractional order (*solid line*) controllers



## 2.6 Introduction to the CRONE Control System Design Methodology

The CRONE (the French acronym for *Commande Robuste d'Ordre Non Entier*, which means fractional order robust control) CSD methodology is a frequency-domain approach that has been developed since the 1980s (Oustaloup 1975, 1981, 1983, 1991, 1995; Oustaloup et al. 1991, 1995, 1999, 2013; Lanusse 1994). It is based on the common unity-feedback configuration presented in Fig. 2.1. Three CRONE CSD methods have been developed, successively extending the field of application. In these three methods the controller or open-loop transfer function is defined using fractional order integro-differentiation. In the frequency domain, they enable linear robust control systems to be simply and methodologically designed.

The major advantage over the  $H_\infty$  design (Vidyasagar and Viswanadham 1982; Francis and Zames 1984) is that the plant uncertainties (or perturbations) are taken into account with no distinction of their nature, whether they are structured (parametric) or unstructured. Unlike  $H_\infty$  controllers, the CRONE controller degree is not the addition of the nominal plant degree, of the perturbation model degree and of the performance filter degree. Using frequency uncertainty domains, as in the Quantitative Feedback Theory approach (QFT) (Horowitz and Sidi 1972; D'Azzo and Houpis 1988; Horowitz 1991, 1993) where they are called templates, the uncertainties (or perturbations) are taken into account in a fully-structured form without overestimation, thus leading to control systems which are as less conservative and thus as high performance as possible. Several benchmarks proposed by Landau have highlighted this property (Landau et al. 1995).

The fractional order, which is either real or complex depending on the generation of the control design, enables parameterization of the open-loop transfer function with a small number of high-level parameters. The optimization of the control is thus reduced to only the search for the optimal values of these parameters. Unlike QFT, CRONE CSD avoids iterative nonlinear optimization of each parameter of the controller's rational transfer function.

The third, and most powerful, CRONE CSD method is able to design controllers for plants with positive real part zeros or poles, time delay, and/or with lightly damped modes. Associated with the w-bilinear variable change, it can also be used to design digital controllers. The CRONE methodology has also been extended to linear time-variant systems and nonlinear systems whose nonlinear behaviors are taken into account by sets of linear equivalent behaviors. For MIMO (multivariable) plants, two methods have been developed. The choice of the method is made through an analysis of the coupling rate of the plant. When this rate is reasonable, one can opt for the simplicity of the multi-SISO approach to design a decentralized controller, whereas when the rate is high, the full MIMO approach of the CRONE methodology has to be used.

A CRONE toolbox has been developed and is freely available for the international scientific community for research and pedagogical purposes (Oustaloup et al. 2000; Melchior et al 2002; Lanusse 2010; Lanusse et al. 2011, 2013). The toolbox

can be used to solve the robust control problems proposed in the following sections. It can be downloaded at <http://www.ims-bordeaux.fr/CRONE/toolbox>.

## 2.7 First Generation CRONE Control System Design

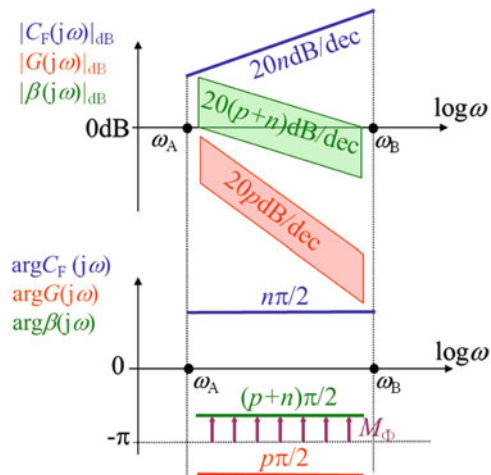
Since the open-loop transfer function of the system presented in Fig. 2.1 is defined by the product of  $G(s)$  and  $C(s)$ , the variations of the phase margin  $M_\Phi$  come both from the parametric variations of the plant (which leads to an uncertain frequency response) and from the controller phase variations over the frequency range where the frequency  $\omega_{cg}$  may vary. The first generation CRONE control proposes to use a controller without phase variation around frequency  $\omega_{cg}$ . This strategy has to be used when the frequency  $\omega_{cg}$  is within a frequency range where the plant phase is constant (with respect to the frequency). In this range where the plant frequency response is asymptotic (this frequency band is called a plant asymptotic-behavior band) the plant variations are only gain-like.

Within a frequency range  $[\omega_A, \omega_B]$  around the desired frequency  $\omega_{cg}$ , the CRONE controller is defined from the fractional transfer function of an order  $n$  integro-differentiator:

$$C_F(s) = C_0 s^n \text{ with } n \text{ and } C_0 \in \mathbb{R}. \quad (2.74)$$

The constant phase  $n\pi/2$  characterizes this controller around frequency  $\omega_{cg}$ . When the plant gain or plant corner frequencies vary (the latter are greatly different from the frequency  $\omega_{cg}$ ), the constant phase controller  $C_F$  does not modify the phase margin (Fig. 2.34). Thus, the frequency range  $[\omega_A, \omega_B]$  must equal the range where the frequency  $\omega_{cg}$  can vary.

**Fig. 2.34** Robustness of the phase margin  $M_\Phi$  provided by a first generation CRONE controller



If the plant asymptotic behavior is an order  $p$  behavior, the phase margin  $M_\Phi$  is:

$$M_\Phi = (n + p + 2) \frac{\pi}{2}. \quad (2.75)$$

In order to make the controller biproper, the fractional order derivative of (2.74) has to be replaced by a band-limited derivative using the corner frequencies  $\omega_l$  and  $\omega_h$ :

$$C_F(s) = C_0 \left( \frac{\omega_l}{\omega_h} \right)^{\frac{n}{2}} \left( \frac{1 + \frac{s}{\omega_l}}{1 + \frac{s}{\omega_h}} \right)^n \text{ with } \omega_l < \omega_A \text{ and } \omega_h < \omega_B. \quad (2.76)$$

Then, to manage the steady state error and the control sensitivity level,  $C_F$  has to be complexified to include an order  $n_l$  band-limited integrator and an order  $n_F$  low-pass filter:

$$C_F(s) = C_0 \left( 1 + \frac{\omega_l}{s} \right)^{n_l} \left( \frac{1 + \frac{s}{\omega_l}}{1 + \frac{s}{\omega_h}} \right)^n \frac{1}{\left( 1 + \frac{s}{\omega_F} \right)^{n_F}}. \quad (2.77)$$

This first generation CRONE controller is obviously very close to the fractional order  $\text{PID}^\mu$  controller defined by (2.69) and  $n_l$  and  $n_F$  are defined in the same way. The main difference is that  $\omega_l$ ,  $\omega_1$ ,  $\omega_h$  and  $\omega_F$  have to be such that a constant phase is achieved on a frequency range  $[\omega_A, \omega_B]$  which covers the frequency range where  $\omega_{cg}$  could vary. Then, the fractional order  $n$  and gain  $C_0$  have to ensure the required nominal phase margin  $M_\Phi$  and open-loop gain crossover frequency  $\omega_{cg}$ :

$$n = \frac{-\pi + M_\Phi - \arg G(j\omega_{cg}) + n_F \arctan \frac{\omega_{cg}}{\omega_F} + n_l \left( \frac{\pi}{2} - \arctan \frac{\omega_{cg}}{\omega_l} \right)}{\arctan \frac{\omega_{cg}}{\omega_l} - \arctan \frac{\omega_{cg}}{\omega_h}} \quad (2.78)$$

and

$$C_0 = \frac{\left( 1 + \frac{\omega_{cg}^2}{\omega_F^2} \right)^{\frac{n_F}{2}}}{|G(j\omega_{cg})| \left( \frac{\omega_h}{\omega_l} \right)^{\frac{n}{2}} \left( 1 + \frac{\omega_l^2}{\omega_{cg}^2} \right)^{\frac{n_l}{2}}}. \quad (2.79)$$

Finally, the first generation CRONE controller can be implemented using a rational transfer function obtained by using Oustaloup's approximation method (Oustaloup 1981) and recursive zeros and poles:

$$C_R(s) = C_0 \left( 1 + \frac{\omega_l}{s} \right)^{n_l} \prod_{i=1}^N \frac{1 + \frac{s}{\omega'_i}}{1 + \frac{s}{\omega_i}} \frac{1}{\left( 1 + \frac{s}{\omega_F} \right)^{n_F}}, \quad (2.80)$$

where

$$\omega'_1 = \sqrt{\eta} \omega_l, \omega_1 = \alpha \omega'_1, \omega'_{i+1} = \alpha \eta \omega'_i \text{ and } \omega_{i+1} = \alpha \eta \omega_i, \quad (2.81)$$

with

$$\alpha = \left( \frac{\omega_h}{\omega_l} \right)^{\frac{n}{N}} \text{ and } \eta = \left( \frac{\omega_h}{\omega_l} \right)^{\frac{1-n}{N}}. \quad (2.82)$$

### ■ Example 2.7

Let us consider again the plant  $G$  defined by (2.49) with an uncertainty on the time constant  $\tau$  :

$$G(s) = \frac{k}{s(1+\tau s)} \text{ with } k = 10 \text{ and } 1000/3 \leq \tau \leq 3 * 1000. \quad (2.83)$$

The requirements remain an open-loop gain crossover frequency  $\omega_{cg}$  about 5 rad/s, a phase margin  $M_\phi$  of  $50^\circ$ , an integrator and a low-pass effect in the controller.

Figure 2.35 presents the Bode diagram of  $G$  for three values of the plant time constant  $\tau$ . Around 5 rad/s, the plant phase is constant whereas its magnitude is uncertain. As it leads to the mean magnitude value, the time constant  $\tau = \tau_{nom} = 1,000$  s is chosen to define the nominal plant  $G_{nom}$ . At  $\omega = 5$  rad/s, the uncertainty of the plant frequency response is 19.1 dB for the magnitude and  $0.03^\circ$  for the phase. Taking into account the required phase margin (and thus the desired rate of decrease in the open-loop magnitude, the open-loop gain crossover frequency can vary from about 2.3 to 11 rad/s (explained below). Within this frequency range, the nominal plant phase varies by  $0.06^\circ$  at least. Thus the first generation CRONE CSD method can be used to obtain a robust controller.

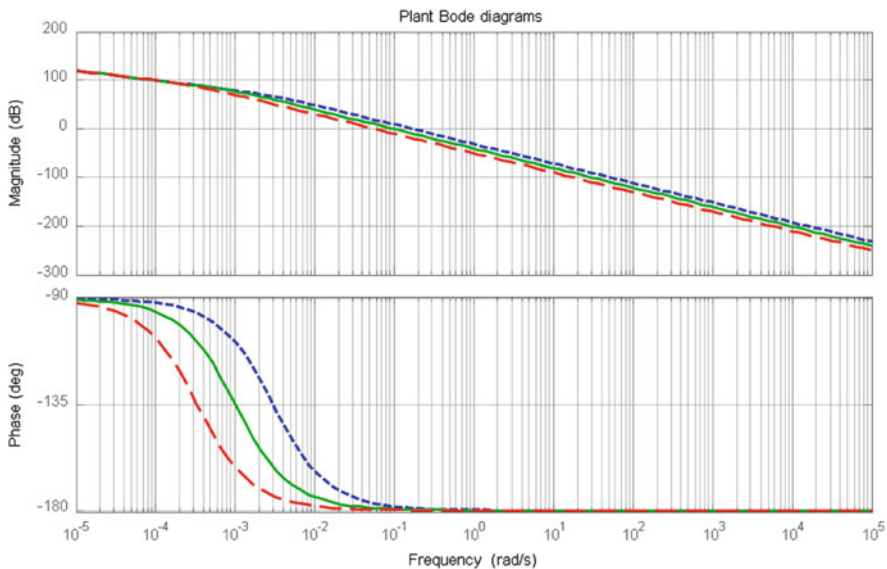


**Fig. 2.35** Plant Bode diagram for the 3 values of  $\tau$ :  $\tau = \tau_{nom}/3$  (---),  $\tau = \tau_{nom}$  (—) and  $\tau = \tau_{nom} * 3$  (---

From (2.75) it follows that:

$$n + p = \frac{50}{90} - 2 = -1.44. \quad (2.84)$$

From the rate of decrease in the open-loop magnitude gain and from the plant magnitude uncertainty, in order to ensure the robustness of the phase margin, the frequency range  $[\omega_A, \omega_B]$  needs to cover 0.66 decade:

$$\log_{10} \frac{\omega_B}{\omega_A} = \left| \frac{19.1}{20(n+p)} \right| = 0.66 \text{ then } \frac{\omega_B}{\omega_A} = 10^{0.66} = 4.62. \quad (2.85)$$

As the nominal plant leads to the mean magnitude of the open-loop frequency response around 5 rad/s:

$$\omega_A = \omega_{cg \text{ nom}} / \sqrt{4.62} = 2.33 \text{ rad/s and } \omega_B = \omega_{cg \text{ nom}} \sqrt{4.62} = 10.7 \text{ rad/s.} \quad (2.86)$$

In order to achieve a constant phase the corner frequencies  $\omega_l$  and  $\omega_h$  are set to:

$$\omega_l = \omega_A / 10 = 0.233 \text{ rad/s and } \omega_h = 10\omega_B = 107 \text{ rad/s.} \quad (2.87)$$

As  $n_l$  and  $n_F$  are set to 1, to avoid damage to the constant phase, the corner frequencies  $\omega_l$  and  $\omega_F$  are set to:

$$\omega_l = \omega_{cg \text{ nom}} / 40 = 0.125 \text{ rad/s and } \omega_F = 40\omega_{cg \text{ nom}} = 200 \text{ rad/s.} \quad (2.88)$$

It is about  $\omega_l/2$  for  $\omega_l$  and  $2\omega_h$  for  $\omega_F$ . As  $|G(j5)| = 4.10^{-4}$  and  $\arg G(j5) = -180^\circ$ , using (2.78) and (2.79), the nominal phase margin and open-loop gain crossover frequency are ensured with:

$$n = 0.624 \text{ and } C_0 = 368. \quad (2.89)$$

Thus the fractional order CRONE controller is:

$$C(s) = 368 \left( 1 + \frac{0.125}{s} \right) \left( \frac{1 + \frac{s}{0.233}}{1 + \frac{s}{107}} \right)^{0.624} \frac{1}{1 + \frac{s}{200}}. \quad (2.90)$$

Figure 2.36 compares the Bode diagrams of the PID controller defined by (2.50) and of the CRONE controller. Even if their gain and phase are the same at the required nominal open-loop gain crossover frequency (5 rad/s), the Bode diagrams show that the CRONE controller provides a (close to) constant phase around this frequency. The low-frequency gain is lower, while the high-frequency gain is higher for the CRONE controller than for the PID controller.

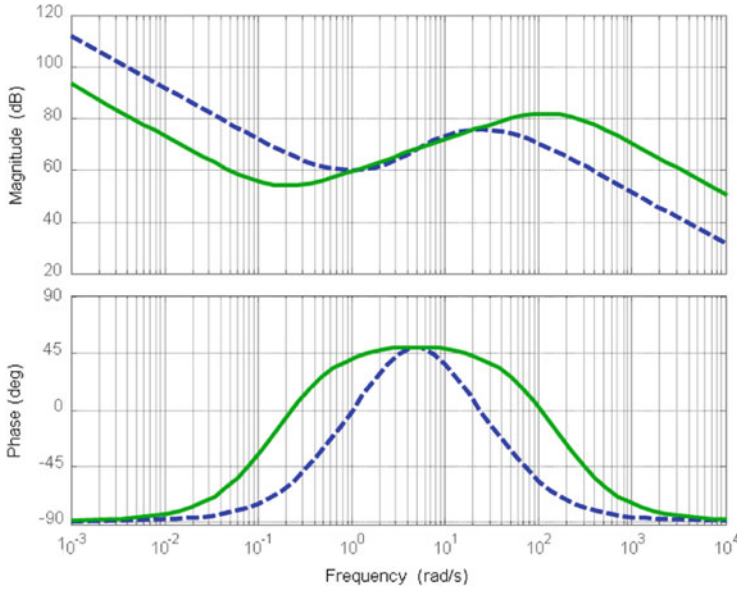


**Fig. 2.36** Comparison of the Bode diagram of the integer order controller (*dashed line*) and of the fractional order CRONE controller (*solid line*)

For the 3 parametric states of the plant, Figs. 2.37 and 2.38 present respectively the open-loop Nichols and Nyquist plots. Figure 2.38 clearly shows the constant phase of the open-loop frequency response when its magnitude is close to one.

Even when  $\tau$  is perturbed, the CRONE open-loop frequency response shows that the phase and gain margins can be no less than  $48^\circ$  and 30 dB. The gain crossover frequency varies from 2.26 to 11.1 rad/s. Furthermore the Nichols chart magnitude contours indicate that the resonance peak of  $T$  does not vary a lot; its highest value never exceeds 2.87 dB. The phase margin and resonance peak of  $T$  can be absolutely constant if the band-limitation effected by  $\omega_l$  and  $\omega_h$  is less severe. However, this can lead to higher values of the magnitude of the  $CS$  and  $SG$  sensitivity functions. Our choice permits a good management of the performance/robustness tradeoff. Figure 2.39 presents the closed-loop sensitivity functions. It shows that:

- even if the nominal resonant peak of  $T$  is 2.34 dB, it reaches only 2.87 dB when  $G$  is perturbed;
- the resonant peaks of  $S$  are the same of those of  $T$ , thus the modulus margin is always greater than 0.75;
- $T$  is close to 0 dB (accurate tracking of reference signal) and  $S$  is small (good desensitization) up to 1 rad/s;
- $SG$  decreases (efficient rejection of input disturbance) when  $\omega$  decreases from 0.2 rad/s;
- $CS$  reaches about 82 dB at 100 rd/s and then decreases (low amplification of noise measurement).

**Fig. 2.37** CRONE open-loop Nichols plot for the 3 values

of  $\tau$ :  $\tau = \tau_{\text{nom}}/3$  (---),  $\tau = \tau_{\text{nom}}$  (—) and  $\tau = \tau_{\text{nom}} * 3$  (---

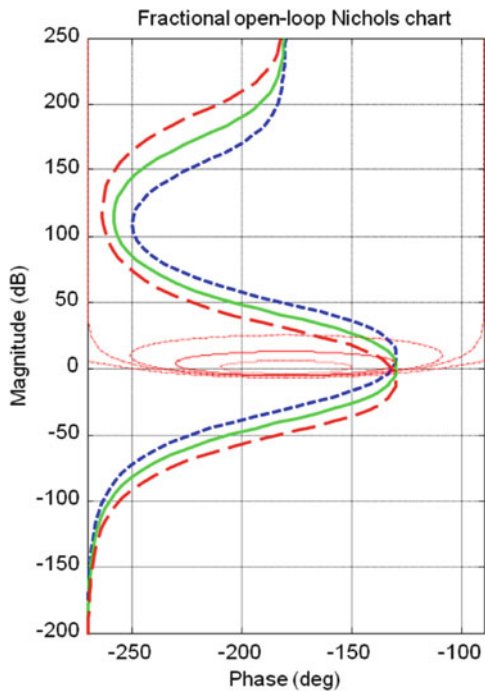
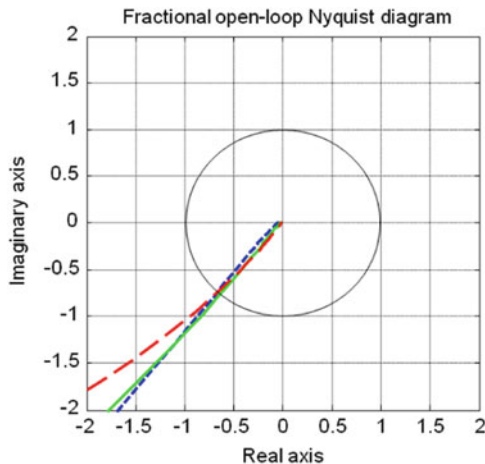


**Fig. 2.38** CRONE open-loop Nyquist locus for the 3 values

of  $\tau$ :  $\tau = \tau_{\text{nom}}/3$  (---),  $\tau = \tau_{\text{nom}}$  (—) and  $\tau = \tau_{\text{nom}} * 3$  (---



As the frequency range  $[\omega_l, \omega_h]$  covers three decades,  $N = 4$  suffices to approximate the fractional order part that appears in (2.90). The recursive ratios are defined by:

$$\alpha = 2.61 \text{ and } \eta = 1.78. \quad (2.91)$$

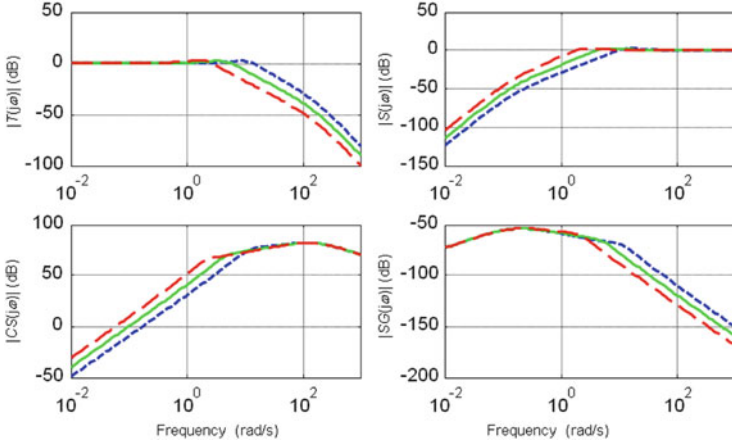


**Fig. 2.39** CRONE closed-loop sensitivity functions for the 3 values of  $\tau$ :  $\tau = \tau_{\text{nom}}/3$  (---),  $\tau = \tau_{\text{nom}}$  (—) and  $\tau = \tau_{\text{nom}}*3$  (-.-)

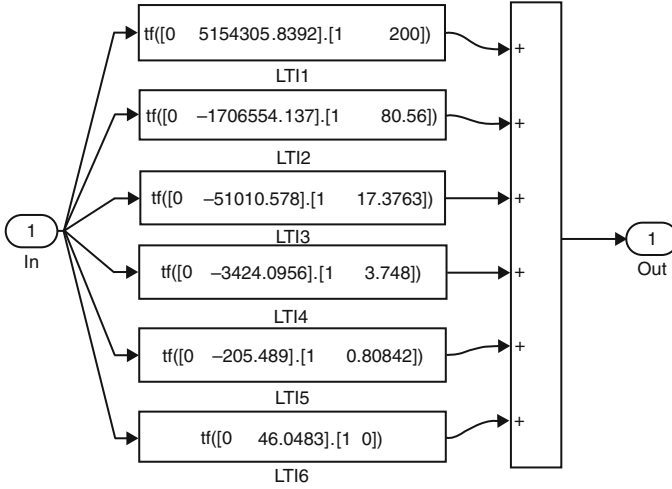


**Fig. 2.40** Parallel form of the designed CRONE controller

Then the first generation CRONE controller to be implemented is:

$$C_R(s) = 368 \left( 1 + \frac{0.125}{s} \right) \frac{1 + \frac{s}{0.310}}{1 + \frac{s}{0.808}} \frac{1 + \frac{s}{1.44}}{1 + \frac{s}{3.75}} \frac{1 + \frac{s}{6.67}}{1 + \frac{s}{17.4}} \frac{1 + \frac{s}{30.9}}{1 + \frac{s}{80.6}} \frac{1}{1 + \frac{s}{200}}. \quad (2.92)$$

To avoid numerical problems, such a controller can be implemented using a parallel form obtained from a partial-fraction expansion. Figure 2.40 shows the controller model provided by the CRONE CSD toolbox.



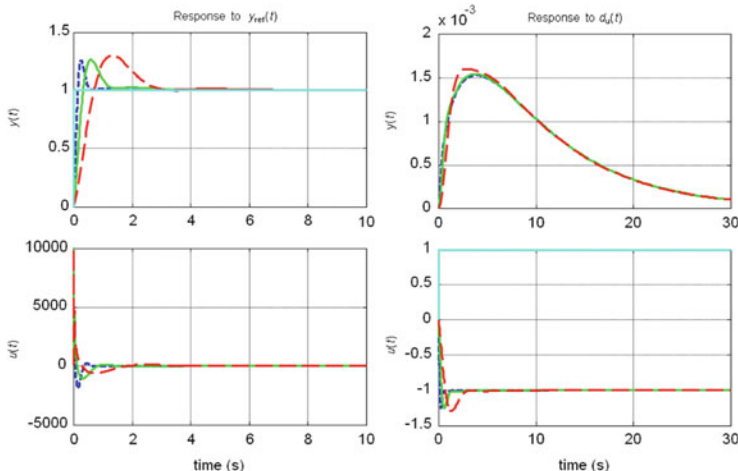


**Fig. 2.41** CRONE closed-loop step responses for the 3 values of  $\tau$ :  $\tau = \tau_{\text{nom}}/3$  (---),  $\tau = \tau_{\text{nom}}$  (—) and  $\tau = \tau_{\text{nom}}*3$  (—)

Figure 2.41 presents the step responses of the closed-loop system. It shows that:

- for long durations, the tracking of  $y_{\text{ref}}$  and the rejection of  $d_u$  are efficient;
- unlike the PID controller defined by (2.50), the CRONE controller provides a percentage overshoot for the response of  $y$  to  $y_{\text{ref}}$  that remains almost constant;
- the response of  $u$  to  $y_{\text{ref}}$  quickly reaches 10,000, two times the level obtained with the PID controller;
- the response of  $y$  to  $d_u$  remains well damped when  $\tau$  is perturbed even if it requires 30 s to reject the disturbance (8 s for the PID).

To sum up, this CRONE controller is robust even if it requires a greater control level and takes longer to reject an input disturbance. It illustrates perfectly the robustness/performance tradeoff.  $\square$

## 2.8 Conclusion

This chapter has presented the Control System Design of a controller using the frequency-domain approach. It focused on PID, fractional order PID and then first generation CRONE controllers. Fractional order controllers provide more tuning parameters that are used to improve robustness by the CRONE methodology. The first generation CRONE controllers can be used for plants with magnitude variation and constant phase. When the plant phase varies with respect to the frequency, the second generation of CRONE controllers can be used. As described in the following chapter, this robust controller is designed through a fractional order open-loop transfer function. From real, the order will become complex for both gain and phase perturbed plants. This will define the third generation CRONE methodology.

## References

- Cervera J, Baños A (2006) Tuning of fractional PID controllers by using QFT. In: Proceedings of IECON'06 – 32nd annual conference of the IEEE industrial electronics society, Paris
- Chen YQ, Moore KL, Vinagre B, Podlubny I (2004) Robust PID controller auto tuning with a phase shaper. In: Proceedings of The first IFAC symposium on fractional differentiation and its applications (FDA04), Bordeaux
- D'Azzo JJ, Houpis CH (1988) Linear control system analysis and design, conventional and modern. McGraw Hill, New York
- Francis BA, Zames G (1984) On  $H_\infty$  optimal sensitivity theory for SISO feedback systems. IEEE Trans Autom Control 29:9–16
- Goodwin GC, Graebe SF, Salgado ME (2001) Control system design. Prentice Hall, New Jersey
- Horowitz IM, Sidi M (1972) Synthesis of feedback systems with large plant ignorance for prescribed time-domain tolerances. Int J Control 16:287–309
- Horowitz IM (1991) Survey of quantitative feedback theory (QFT). Int J Control 53:255–291
- Horowitz IM (1993) Quantitative feedback design theory – QFT. QFT Publications, Boulder
- Kochenburger RJ (1950) A frequency response method for analyzing and synthesizing contactor servomechanisms. Trans AIEE (Am Inst Electr Eng) 69(1):270–284
- Krylov NM, Bogoliubov N (1943) Introduction to nonlinear mechanics. Princeton University Press, Princeton. ISBN 0691079854
- Landau ID, Rey D, Karimi A, Voda A, Franco A (1995) A flexible transmission system as a benchmark for digital control. Eur J Control 1(2):77–96
- Lanusse P (1994) De la commande CRONE de 1ère generation à la commande CRONE de 3ème generation. Ph.D. thesis, Université Bordeaux 1
- Lanusse P (2010) CRONE control system design, a CRONE toolbox for Matlab. <http://www.ims-bordeaux.fr/CRONE/toolbox>
- Lanusse P, Oustaloup A (2005) Anti-windup system for 1st generation crone controller. In: Ubooks (ed) Fractional differentiation and its applications, vol 3, Systems analysis, implementation and simulation, systems identification and control. Ubooks, Neusäss, pp 191–204
- Lanusse P, Oustaloup A, Sabatier J (2007) Robust design of an anti-windup compensated 3rd generation CRONE controller. In: Sabatier J, Agrawal OP, Tenreiro Machado JA (eds) Advances in fractional calculus: theoretical developments and applications in physics and engineering. Springer, Dordrecht, pp 527–542
- Lanusse P, Sabatier J, Oustaloup A (2010) Design of controllers using damping contours defined from closed loop systems based on fractional complex order integrators. In: ASME/IEEE international conference on mechatronic and embedded systems and applications (MESA10), QingDao
- Lanusse P, Malti R, Melchior P (2011) CRONE control-system design toolbox for the control engineering community. In: ASME/IEEE international conference on mechatronic and embedded systems and applications, Washington, DC
- Lanusse P, Oustaloup A, Pommier-Budinger V (2012) Stability of closed-loop fractional-order systems and definition of damping contours for the design of controllers. Int J Bifurcat Chaos 22(4). doi: [10.1142/S0218127412300133](https://doi.org/10.1142/S0218127412300133)
- Lanusse P, Malti R, Melchior P (2013) Crone control system design toolbox for the control engineering community: tutorial and a case study. Philos Trans Royal Soc A, 371(1990):20120149. doi: [10.1098/rsta.2012.0149](https://doi.org/10.1098/rsta.2012.0149)
- Maamri N, Trigeassou JC, Tenoutit M (2010) On fractional PI and PID controllers. In: Proceedings of the FDA 2010 IFAC Workshop, Badajoz
- Manabe S (1960) The non-integer integral and its application to control systems. ETJ Japan 6(3/4):83–87
- Manabe S (1961) The non integer integral and its application to control systems. ETJ Japan 6(3–4):83–87

- Melchior P, Lanusse P, Cois O, Dancla F, Oustaloup A (2002) Crone Toolbox for Matlab: fractional systems toolbox. Tutorial workshop on “fractional calculus applications in automatic control and robotics”. In: 41st IEEE CDC’02, Las Vegas
- Monje CA, Vinagre B, Chen YQ, Feliu V, Lanusse P, Sabatier J (2004) Proposals for fractional  $PI^\lambda D^\mu$  tuning. In: Proceedings of the first IFAC symposium on fractional differentiation and its applications (FDA04), Bordeaux
- Monje CA, Chen Y, Vinagre BM, Xue D, Feliu-Batlle V (2010) Fractional-order systems and controls: fundamentals and applications. Springer, London\New York
- Nataraj PSV, Tharewal S (2010) On fractional-order QFT controllers. Trans ASME J Dynamic Syst Meas Control 129:212–218
- Oustaloup A (1975) Etude et réalisation d’un système d’asservissement d’ordre 3/2 de la fréquence d’un laser à colorant continu. Ph.D. thesis, Université Bordeaux 1, France
- Oustaloup A (1981) Linear feedback control systems of fractional order between 1 and 2. In: The IEEE international symposium on circuits and systems, Chicago, Illinois
- Oustaloup A (1983) Systèmes asservis linéaires d’ordre fractionnaire. Ed Masson, Paris
- Oustaloup A (1991) La commande CRONE. Edition Hermès, Paris
- Oustaloup A (1995) La dérivation non entière, théorie, synthèse et applications. Editions Hermès, Paris
- Oustaloup A, Ballouk A, Lanusse P (1991) Synthesis of a narrow band template based on complex non integer derivation. In: IMACS symposium “modelling and control of technological systems”, Lille
- Oustaloup A, Lanusse P, Mathieu B (1995) Robust control of SISO plants : the CRONE control. In: ECC’95, Rome
- Oustaloup A, Sabatier J, Lanusse P (1999) From fractal robustness to the CRONE control. Fractional Calc Appl Anal 2(1):1–30
- Oustaloup A, Melchior P, Lanusse P, Cois O, Dancla F (2000) The CRONE toolbox for Matlab. In: IEEE international symposium on computer-aided control system design, Anchorage
- Oustaloup A, Pommier V, Lanusse P (2003) Design of a fractional control using performance contours – application to an electromechanical system. Fractional Calc Appl Anal Int J Theory Appl 6(1):1–24
- Oustaloup A, Lanusse P, Sabatier J, Melchior P (2013) CRONE control : principles, extensions and applications. J Appl Nonlin Dyn 2(3):207–223. doi:[10.5890/JAND.2013.08.001](https://doi.org/10.5890/JAND.2013.08.001)
- Petras I (1999) The fractional-order controllers: methods for their synthesis and application. J Electr Eng 50(9–10):284–288
- Podlubny I (1999) Fractional-order systems and  $PI^\lambda D^\mu$ -controllers. IEEE Trans Autom Control 44(1):208–214
- Pommier-Budinger V, Janat Y, Nelson-Gruel D, Lanusse P, Oustaloup A (2008) Fractional robust control with iso-damping property. In: American control conference 2008, Seattle
- Popov VM (1962). Absolute stability of nonlinear systems of automatic control, Automation and Remote control, (Russian original in 1961), pp 857–875
- Tustin A (1958) The design of systems for automatic control of the position of massive object. Proc Inst Electr Eng 105C(1):1–57
- Valerio D, Sa da Costa J (2012) An introduction to fractional control. IET Editor, Institution of Engineering and Technology
- Vidyasagar M, Viswanadham N (1982) Algebraic design techniques for realizable stabilisation. IEEE Trans AC 27(5):895–903
- Wurmthaler C, Hippe P (1991) Systematic compensator design in the presence of input saturation. In: Proceeding of ECC’91, Grenoble
- Ygorra S, Cazaurang F, Bergeon B (1996) Anti windup control of stable plants with input saturation. In: Proceeding of CESA’96, Lille

Fractional Order Differentiation and Robust Control  
Design

CRONE, H-infinity and Motion Control

Sabatier, J.; Lanusse, P.; Melchior, P.; Oustaloup, A.

2015, IX, 323 p. 349 illus., 150 illus. in color., Hardcover

ISBN: 978-94-017-9806-8